THE JOURNAL OF PHYSICAL CHEMISTRY B

Article

pubs.acs.org/JPCB

Vibrational Stark Effects of Carbonyl Probes Applied to Reinterpret IR and Raman Data for Enzyme Inhibitors in Terms of Electric Fields at the Active Site

Samuel H. Schneider and Steven G. Boxer*

Department of Chemistry, Stanford University, Stanford, California 94305-5012, United States

Supporting Information

ABSTRACT: IR and Raman frequency shifts have been reported for numerous probes of enzyme transition states, leading to diverse interpretations. In the case of the model enzyme ketosteroid isomerase (KSI), we have argued that IR spectral shifts for a carbonyl probe at the active site can provide a connection between the active site electric field and the activation free energy (Fried et al. *Science* **2014**, *346*, 1510−1514). Here we generalize this approach to a much broader set of carbonyl probes (e.g., oxoesters, thioesters, and amides), first establishing the sensitivity of each probe to an electric field using vibrational Stark spectroscopy, vibrational solvatochromism, and MD simulations, and then applying these results to reinterpret data already in the literature for enzymes such as 4-chlorobenzoyl-CoA dehalogenase and serine proteases. These results demonstrate that the vibrational Stark effect provides a general framework for estimating the electrostatic contribution to the catalytic rate and may provide a metric for the design or modification of enzymes. Opportunities and limitations of the approach are also described.

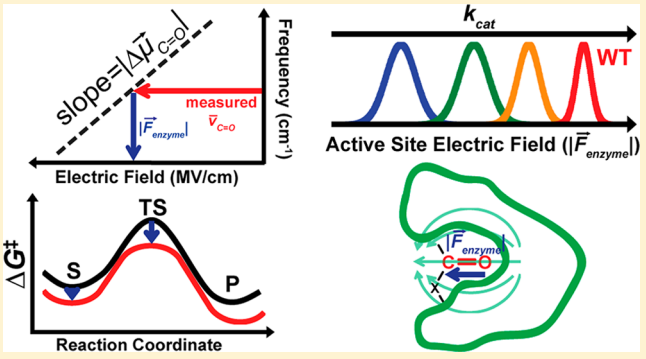

INTRODUCTION

The physical origins of the remarkable catalytic properties of enzymes have been the subject of intense interest in many laboratories. We have recently provided a framework for extracting information on the electrostatic contribution to the catalytic rate of the model enzyme ketosteroid isomerase (KSI) by using the vibrational Stark effect (VSE).[1] While many laboratories using well-chosen inhibitors as probes have obtained a large body of high quality infrared and Raman data, the absence of a physically based interpretation of the observed spectral shifts and their relationship to the catalytic rate has led to considerable confusion. In this paper, we extend the application of the VSE approach to the analysis of vibrational data in the literature for several other enzymes, suggesting that this approach is generalizable, and also noting its limits.

The vibrational Stark effect is a relatively new method to probe electric fields in condensed matter. Vibrational Stark spectroscopy (VSS) in a defined external electric field, $\vec{F}_{ext}$, provides a calibration step quantifying the sensitivity of a vibrational transition to an electric field, known as the Stark tuning rate or difference dipole for the probe oscillator, $|\Delta\vec{\mu}_{probe}|$, expressed in units of $cm^{-1}/(MV/cm)$. The VSE is then the more general application of such a calibrated vibrational probe to obtain information on the absolute electric field (MV/cm)

$$\Delta\bar{\nu}_{obs} = -\Delta\vec{\mu}_{probe}\cdot\vec{F}_{matrix} \quad (1)$$

where $\Delta\bar{\nu}_{obs}$ is the observed vibrational frequency shift (in cm^{-1}) from a reference state calibrated to zero electric field and $\vec{F}_{matrix}$ is the electric field experienced by the vibrational probe due to a particular environment or matrix. For localized bond modes, the angle between $\Delta\vec{\mu}_{probe}$ and the transition dipole moment is expected to be zero, as has been confirmed in several cases, and since the transition dipole for high frequency vibrational modes is typically parallel to the oscillator bond axis, the direction of $\Delta\vec{\mu}_{probe}$ in a complex system like a protein is known by X-ray crystallography.[2] As such, these vibrational modes serve as calibrated and directional probes of the projection of the electric field exerted by the environment along the bond axis. Furthermore, vibrational solvatochromism can be used to systematically vary the field experienced by the probe in fluid solution, and the resulting spectral shifts can be related to the absolute electric field through MD simulations.[3−5] The separately measured Stark tuning rate (by VSS) provides a bridge between these two approaches. Additional computational methods have also been developed to determine the environmental effects on vibrational frequencies.[6−10] A key assumption is that $|\Delta\vec{\mu}_{probe}|$ is unaffected by $\vec{F}_{matrix}$; that is, spectral shifts are interpreted entirely as being due to a classical

Received: August 11, 2016
Revised: August 19, 2016
Published: August 19, 2016

DOI: 10.1021/acs.jpcb.6b08133
J. Phys. Chem. B 2016, 120, 9672−9684

Table 1. Enzymatic Systems Where Perturbed Carbonyl Frequencies Have Been Reported from IR and Raman Spectroscopy

enzyme	vibrational probe
triosephosphate isomerase (TIM)[26]	dihydroxyacetone phosphate (ketone)
β-lactamase[32−35]	β-lactam antibiotics (amide/ester)
fructose-1,6-bisphosphate aldolase[27]	glyceraldehyde-3-phosphate (aldehyde)
citrate synthase[28]	oxaloacetate (ketone)
alcohol dehydrogenase[36]	*N*-cyclohexylformamide (amide)
serine proteases[29,37−40]	(5-methylthienyl)acrylate (ester)
chorismate mutase[41]	prephenate (ketone)
lactate dehydrogenase[30,42]	pyruvate (ketone)
enoyl-CoA hydratase (crotonase)[43]	cinnamoyl-CoA (thioester)
cysteine proteases[44]	(5-methylthienyl)acrylate (thioester)
4-chlorobenzoyl-CoA dehalogenase[45,46]	4-methylbenzoyl-CoA (thioester)
DD-transpeptidase[47]	β-lactam antibiotics (amide/ester)
uracil DNA glycosylase[48]	2-β-fluorodeoxyuridine (amide)
ketosteroid isomerase[1,49]	19-nortestosterone (enone)

electrostatic interaction, not a change in the probe vibration's bond order. We return to this assumption later.

The nitrile (C≡N) vibration has been widely used due to its absorption in an uncluttered region of the IR spectrum.[11−15] However, the nitrile probe's electrostatic response is complicated by other effects in hydrogen bonding (H-bonding) solvents.[16−19] The carbonyl (C═O) vibration, which is generally more intense than nitriles, has been shown to vary linearly with electrostatic field in both H-bonding and non-H-bonding environments.[3,5,7,8,20] The main limitation of the carbonyl probe is that its frequency overlaps with the densely populated amide I region in many biological systems. Fortunately, this can often be overcome by careful selection of a reference sample that is nearly identical to the sample of interest as well as isotopic labeling, or by using Raman spectroscopy. The earliest work used CO bound to the heme iron of myoglobin mutants,[21,22] and this has recently been extended by us to acetophenone and the carbonyl group on 19-nortestosterone, an inhibitor of KSI, to provide an estimate for the electric field in the active site and its contribution to lowering the activation free energy.[1,23]

There already exists a large body of work describing perturbed carbonyl frequency shifts in the active site of enzymes, several of which document a relationship between the catalytic rate and C═O frequency; some examples are listed in Table 1. These findings have been the subject of diverse interpretations including but not limited to bond polarization, distortion, and ground-state destabilization.[24−31] We believe that the VSE can provide a more general, consistent, and quantitative framework with which to interpret these findings and explore the role of electric fields in catalysis.

In order to expand the applications of the carbonyl vibrational probe to diverse problems, we report experimental Stark tuning rates for various oxoesters, thioesters, and amides of biologically relevant model compounds. Additionally, we measure vibrational solvatochromism for these probes and use MD simulations to calculate absolute electric fields, finding that all exhibit a linear field-frequency relationship. These results, summarized in part A of the Results and Discussion, should be useful for further studies using carbonyl probes, following in the same spirit as an earlier paper on VSS of diverse oscillator types.[50] We follow this in part B by reinterpreting IR and Raman data obtained by others for several enzymes in terms of the vibrational Stark effect to quantify the contributions of electric fields to catalysis.

MATERIALS AND METHODS

The carbonyl-containing compounds were acquired from the following sources: *N*,*N*-dimethylacetamide (DMA, 99.9%, Sigma-Aldrich), *N*-methylacetamide (NMA, 99% Sigma-Aldrich), *S*-butyl thiobenzoate (>95%, TCI America), ethyl thioacetate (98%, Sigma-Aldrich), ethyl acetate (99.8%, Sigma-Aldrich), methyl acetate (>98%, Sigma-Aldrich), methyl propionate (>98%, Sigma-Aldrich), methyl benzoate (99%, Sigma-Aldrich), methyl *trans*-cinnamate (99%, Sigma-Aldrich), ethyl 4-aminocinnamate (97%, Sigma-Aldrich), ampicillin sodium salt (Sigma-Aldrich), β-nicotinamide adenine dinucleotide 2′-phosphate reduced tetrasodium salt (NADPH, 95%, Sigma-Aldrich). Solvents were purchased as follows: 2-methyltetrahydrofuran (2MeTHF, >99%, Sigma-Aldrich), toluene (99.8%, Sigma-Aldrich), ethanol (99.5%, Acros Organics), methanol (99.9%, Fisher Scientific), D_2O (99.8% atom D, Cambridge Isotope), glycer(ol-d_3) (99% atom D, Sigma-Aldrich), ethylene glycol-$(OD)_2$ (98% atom D, Sigma-Aldrich). All reagents were used without further purification.

Vibrational Stark Spectroscopy. Carbonyl-containing solutes were dissolved in glass forming solvents as specified for each experiment with typical concentrations of 50−200 mM. Solutions were then loaded in a sample-cell consisting of two offset CaF_2 optical windows (1 mm thickness, 12.7 mm diameter, FOCtek Photonics) coated with a 4.5 nm layer of nickel metal and separated by approximately 26 μm Teflon spacers. The filled sample cell is then immediately immersed into liquid N_2 in a custom-built cryostat,[51] and Stark spectra were recorded on a Bruker Vertex 70 with fields of 0.5−1.8 MV/cm (applied voltages of ca. 1.5−4.0 kV) from a Trek 10/10 high-voltage power amplifier, 1 cm^{-1} resolution, 64 scans apiece of field-on/off transmission spectra, and repeated with increasing fields to ensure the intensity of the Stark spectra scales linearly with the square of the field strength as expected for an isotropic sample.[52] The linear Stark tuning rates were determined as previously described from the second derivative contribution to the Stark spectrum of numerical fits of the zeroth, first, and second derivative contributions of the best-fit Voigt profile of the experimental absorbance spectrum.[52] This analysis assumes an isotropic, immobilized sample and that the angle (ζ) between $\Delta\vec{\mu}_{probe}$ and the transition dipole is zero; the experimentally set angle (χ) between the incident light polarization and the external electric field direction was 90° as previously described.[52] In cases where overlapping peaks were observed (e.g., where both H-bonding and non-H-

DOI: 10.1021/acs.jpcb.6b08133
J. Phys. Chem. B 2016, 120, 9672−9684

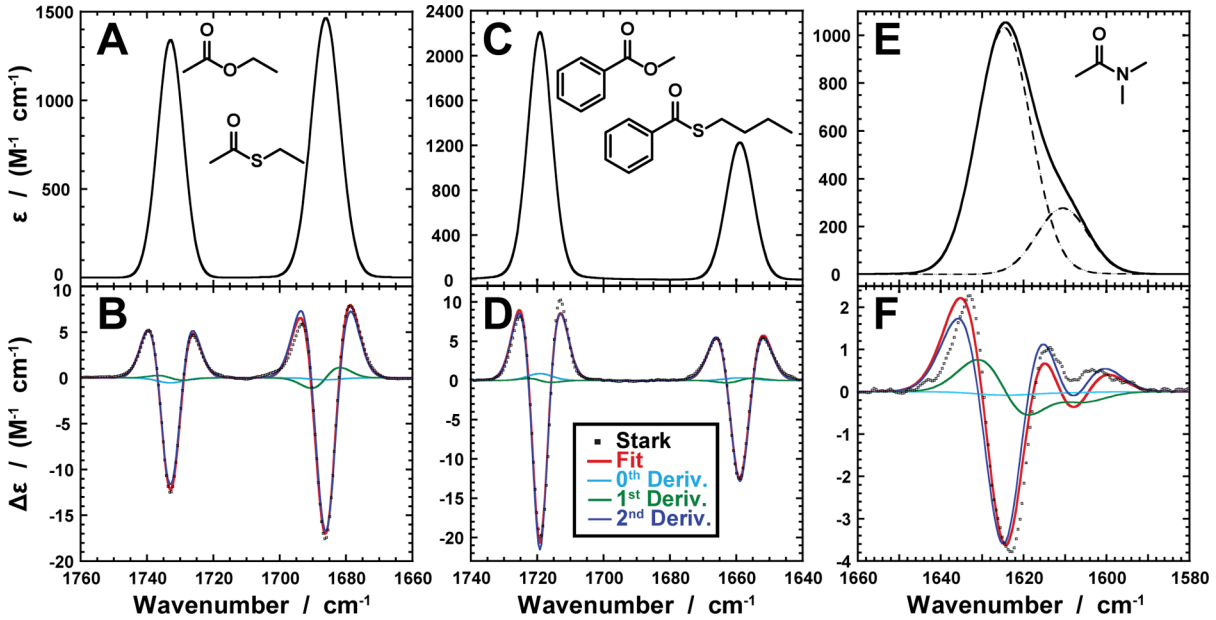

Figure 1. Infrared absorption and Stark spectra for several model carbonyl-containing compounds (see also Figures S1 and S2). The upper panels show infrared absorption spectra, and the lower panels, the corresponding vibrational Stark spectra. (A) The C═O stretch of 100 mM ethyl acetate (left) and ethyl thioacetate (right); (C) methyl benzoate (left) and butyl thiobenzoate (right); (E) *N*,*N*-dimethylacetamide. Parts A–D were obtained in 2-methyltetrahydrofuran, and parts E and F, in ethanol at 77 K. (B, D, and F) The corresponding Stark spectra (■) scaled to an applied field of 1.0 MV/cm with best fits (red) and derivative contributions. The Stark spectrum of *N*,*N*-dimethylacetamide (F) was fit to the derivative contributions of the full absorbance spectrum indicated in part E (solid black trace).

bonding species occur), the derivative contributions were determined from the full absorbance spectrum in the spectral region of interest unless otherwise noted. Note that, while the applied electric field ($\vec{F}_{ext}$) is known accurately from the applied voltage and separation of the electrode, the actual field experienced by the probe ($\vec{F}_{local}$) is modified by the local field correction factor (f), $\vec{F}_{local} = f\vec{F}_{ext}$.[2,52] While the exact value of the local field factor is not known, it is expected to have a value between 1 and 2.[1,4,23,53] As such, the Stark tuning rates are reported in terms of $|\Delta\vec{\mu}_{probe}|f$ and this is discussed in detail with the results.

Vibrational Solvatochromism. FTIR spectra were recorded on a Bruker Vertex 70 spectrometer with a liquid-nitrogen-cooled mercury cadmium telluride (MCT) detector using methods described previously.[3] Briefly, a demountable liquid cell was prepared from two CaF_2 optical windows (0.75 in diameter, 0.25 in thickness, Red Optronics), separated by two semicircular Mylar spacers (75 and 100 μm thickness), to which 20–30 μL of approximately 10 mM solute solution was added.

Transmission spectra were acquired by averaging 128–256 scans after 5–10 min of purging with a nitrogen flow to remove atmospheric CO_2 and water vapor. Spectra were recorded from 2000 to 1400 cm^{-1} with 1 cm^{-1} resolution and aperture settings from 2 to 6 mm in order to maximize signal intensity. The absorption spectra were calculated by taking the negative logarithm of the difference between solute and neat solvent transmission spectra. All solvatochromism measurements were repeated in triplicate, and all frequencies determined using the OPUS software's peak picker (Bruker) as well as Voigt fitting with the Levenberg–Marquardt algorithm.

MD Simulations. All substrate compounds were parametrized first by modeling the molecule in GaussView and then geometry optimized by DFT at the B3LYP/6-311++G(d,p) level in Gaussian 09.[54] The resulting structure was input into the Antechamber program of AmberTools14 and parametrized using the GAFF force field[55,56] and the AM1-BCC method[57] to assign atomic charge parameters. Parameters for organic solvents were taken from Caleman et al.,[58] and water was modeled using the TIP3P parameters.[59] All simulations were set up and carried out in GROMACS version 4.6.5.[60] A single solute molecule was solvated in a cube expanding 2.0 nm around the solute with parametrized solvents as previously described.[3,58] Note that prepolarized, fixed charge force fields were used for these simulations. There are subtle differences when a polarizable force field is used; in particular, the field in hexane is not zero (see ref 4 for a detailed discussion; for the purpose of this work, these much more computationally expensive simulations were not needed).[4] Simulations were performed with periodic boundary conditions, long-range electrostatics were treated by particle-mesh-Ewald (PME) with a 1 nm cutoff, temperature coupling with V-rescale thermostat, and Berendsen pressure coupling. The system was first energy minimized by steepest descent and then equilibrated in the NPT ensemble at 300 K over 200 ps, and finally, MD simulations were carried out for 2.0 ns with snapshots of the forces and positions recorded for a total of 10,000 snapshots per trajectory.

Electric Field Calculations. Electric fields were calculated as previously described.[3] Briefly, using each recorded snapshot from the MD simulations, the forces and positions were calculated on the carbon and oxygen atoms of the carbonyl moiety. Then, a charge-neutralized trajectory was generated keeping all positions at each snapshot constant for both solute and solvent but setting the charge of all solvent atoms to zero. Subtraction of the charge neutralized forces at each snapshot yields the electrostatic forces due to intermolecular solute–solvent interactions. With the forces and positions of each snapshot, the electric field experienced by the carbon and oxygen atoms of the carbonyl were determined by dividing by

DOI: 10.1021/acs.jpcb.6b08133
J. Phys. Chem. B 2016, 120, 9672–9684

Table 2. Vibrational Stark Tuning Rates for Carbonyl-Containing Compounds in Glass-Forming Solvents at 77 K

probe	solvent	peak position (cm^{-1})	fwhm (cm^{-1})	ε_{max} (M^{-1} cm^{-1})[b]	$\lvert\Delta\vec{\mu}_{C=O}\rvert f$ [cm^{-1}/(MV/cm)]
		Oxoesters			
methyl propionate	2MeTHF	1737.75 ± 0.05	9.4 ± 0.1	1166 ± 172	1.05 ± 0.03
methyl acetate	2MeTHF	1738.5	8.90	858	1.06
methyl acetate	ethanol	1741.5	8.9	1380	1.11
ethyl acetate	2MeTHF	1732.9	9.1	1340	1.15
methyl benzoate	2MeTHF	1719.17 ± 0.05	8.7 ± 0.2	1938 ± 300	1.13 ± 0.02
methyl benzoate	4:1 EtOH/MeOH[a]	1721.25 ± 0.05	8.8 ± 0.1	1783 ± 24	1.18 ± 0.03
methyl benzoate	toluene/phenol	1717.7/1697.5	10.0/12.0	1218/287	1.18
methyl *trans*-cinnamate	2MeTHF	1714.2	7.3	1257	1.12
ethyl 4-aminocinnamate	2MeTHF	1699.3	14.2	812	1.48
		Thioesters			
ethyl thioacetate	2MeTHF	1686.05 ± 0.05	10.15 ± 0.05	1450 ± 50	1.47 ± 0.01
butyl thiobenzoate	2MeTHF	1658.9	9.75 ± 0.05	1219 ± 9	1.34 ± 0.01
butyl thiobenzoate	4:1 EtOH/MeOH[a]	1660.25 ± 0.25	10.35 ± 0.05	960 ± 24	1.39 ± 0.03
		Amides			
N,*N*-dimethylacetamide	2MeTHF	1643.6/1628.8/1610.9	11.0/19.6/23.7	630/480/255	1.25
N,*N*-dimethylacetamide	ethanol	1624.7/1610.6	15.2/14.6	1032/277	1.26
N-methylacetamide	2MeTHF	1671.2	8.9	105	1.30
N-methylacetamide[c]	1:1 glycerol/D_2O[a]	1619.5 ± 0.1	21.9 ± 0.1	872 ± 9	1.30 ± 0.01
ampicillin (*β*-lactam)	1:1 glycerol/D_2O[a]	1786.8/1765.5	26.1/14.1	427/122	2.00
ampicillin (*β*-lactam)	3:1 glycerol/D_2O[a]	1765.0	38.1	679	~2.2[d]
ampicillin (amide)[c]	1:1 glycerol/D_2O[a]	1665.9	19.7	167	1.87
ampicillin (amide)[c]	3:1 glycerol/D_2O[a]	1663.9	27.9	398	2.05
NADPH[c]	1:1 ethylene glycol/D_2O[a]	1628.0	16.4	890	0.52

[a]All solvent mixtures are reported as % volume/volume (v/v). [b]All reported ε_{max} represent the extinction coefficient of the Voigt profile that was used in fitting the Stark spectrum. [c]Values correspond to the N-deuterated amides (amide I′). [d]On the basis of the quality of fit, we estimate the Stark tuning rate as 2.2 ± 0.2 cm^{-1}/(MV/cm) based on second derivative analysis, in reasonable agreement with the data in 1:1 glycer(ol-d_3)/D_2O.

the atom's partial charge, and the total electric field experienced by the carbonyl was calculated from the projection of the carbonyl bond vector on the atom's electric field and then averaging the two field projections as previously described.[3] Repeating this for each snapshot of the MD trajectory provides the ensemble-averaged electric field and its standard deviation.[3]

RESULTS AND DISCUSSION

A. VSS, Solvatochromism, and MD Simulations. *Vibrational Stark Spectroscopy.* The vibrational absorption and Stark spectra of several representative oxoesters, thioesters, and amides are shown in Figure 1 along with a larger collection in Figures S1 and S2, and the results are summarized in Table 2. Due to the unique properties of oxoesters and thioesters, the two are easily distinguishable by IR and the Stark spectra of comparably conjugated C=O compounds are shown in Figure 1A–D. By measuring the Stark tuning rates of these different probes simultaneously in the same sample, we minimize any systematic differences in the frozen glass, solvent, and applied field (e.g., voltage and electrode separation), which could affect the local field factor (f), as it is expected to be about the same for a series of compounds in the same solvent.[2,52] At least for cases where there is no band overlap, the Stark spectra are entirely dominated by the second derivative contribution from which $\lvert\Delta\vec{\mu}_{C=O}\rvert f$ is obtained. The local field correction factor, treated here as a scalar, distinguishes the field felt by the probe ($\vec{F}_{local} = f\vec{F}_{ext}$) from the known applied electric field, $\vec{F}_{ext}$, and is a common feature of any spectroscopy that involves the application of electric fields.[23,52,61] While expected to have a value between 1 and 2,[23,62,63] this is a source of uncertainty and our best estimate for its value is discussed further below in the context of comparisons with the solvatochromism data. However, as seen in Table 2, there is negligible variation in the measured Stark tuning rate for a solute across different solvents, suggesting that the local field factor is not a solvent-dependent property. This enables quantitative comparison between different systems for a single probe using the VSE.

In earlier work, the Stark tuning rates of ketones have been observed to be 0.7–1.0 cm^{-1}/(MV/cm), which further increases upon additional conjugation toward values of 1.0–1.8 cm^{-1}/(MV/cm) or greater.[3,22,50] As summarized in Table 2, we observe that $\lvert\Delta\vec{\mu}_{C=O}\rvert f$ has values between 1.05 and 1.48 cm^{-1}/(MV/cm) for various oxoesters, 1.39–1.47 cm^{-1}/(MV/cm) for thioesters, and 0.52–2.2 cm^{-1}/(MV/cm) for the amides studied herein. The results with model oxoesters are in close agreement with that observed by Takashima et al. for poly(methyl methacrylate) films of $\lvert\Delta\vec{\mu}_{C=O}\rvert f$ = 1.06 cm^{-1}/(MV/cm).[64] Pazos et al. predicted the Stark tuning rate for the methyl ester analogues of aspartic and glutamic acid from vibrational solvatochromism and MD simulations, but these were overestimates (1.3 cm^{-1}/(MV/cm)) of those reported in Table 2 for methyl acetate and methyl propionate, likely due to a correction for the local field factor that was implicit in the calculations and carried over from earlier studies with acetophenone.[3,5]

The Stark tuning rates ($\lvert\Delta\vec{\mu}_{C=O}\rvert f$) of *N*-methylacetamide (NMA) and *N*,*N*-dimethylacetamide are both ca. 1.3 cm^{-1}/(MV/cm). Assuming a local field factor of 2, this is in good agreement with the calculated value $\lvert\Delta\vec{\mu}_{C=O}\rvert$ = 0.65 or 0.78 cm^{-1}/(MV/cm) using either a distributed dipole or distributed charge coarse-grained model.[65,66] Recent work by Oh et al.[67] estimates the Stark tuning rate ($\lvert\Delta\vec{\mu}_{C=O}\rvert$) of the amide I mode for a $^{13}C{=}^{18}O$ labeled peptide to be 1.4 cm^{-1}/(MV/cm), which differs by the local field factor. Computational studies[68]

DOI: 10.1021/acs.jpcb.6b08133
J. Phys. Chem. B 2016, 120, 9672–9684

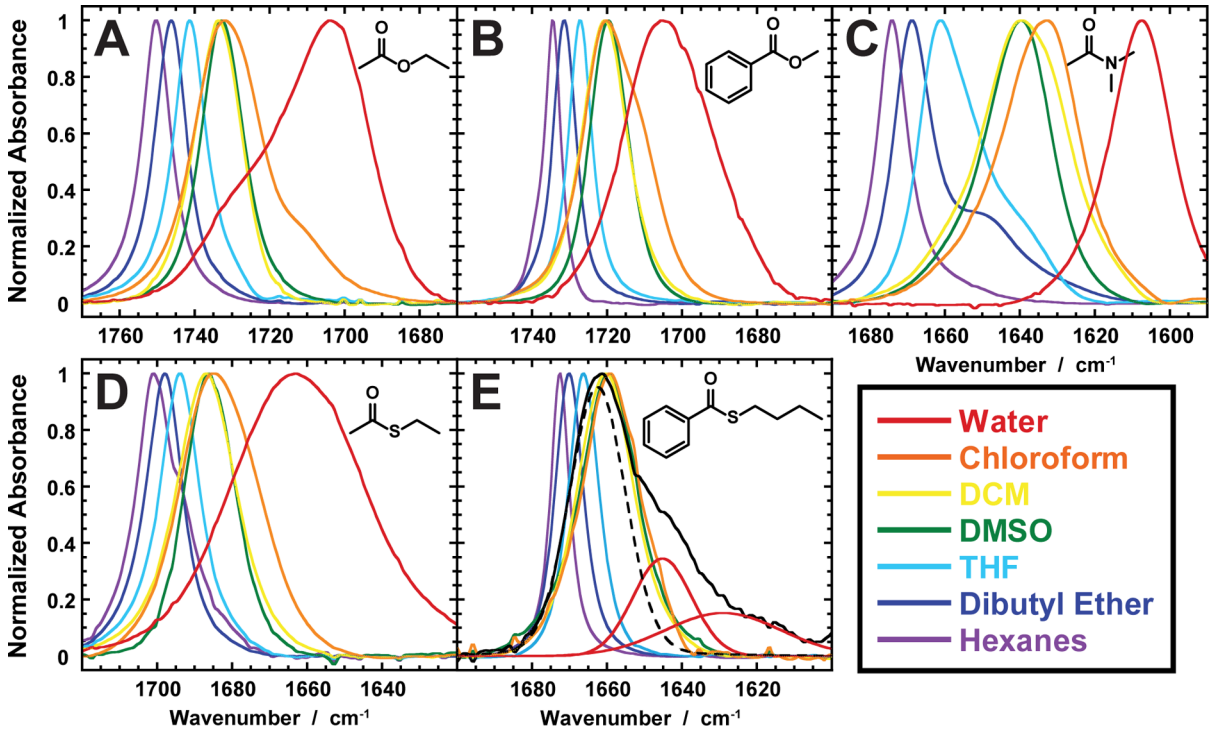

Figure 2. Vibrational solvatochromism of carbonyl-containing compounds. Infrared spectra of the respective carbonyl moiety from 10 mM (A) ethyl acetate, (B) methyl benzoate, (C) *N*,*N*-dimethylacetamide, (D) ethyl thioacetate, and (E) butyl thiobenzoate dissolved in a series of organic solvents of increasing polarity and D_2O. The C═O peaks of butyl thiobenzoate in D_2O (black line) were determined in 1:2 (% v/v) DMSO/D_2O due to poor solubility, and the broad feature decomposed into three peaks corresponding to the carbonyl in DMSO (1662.6 ± 0.1 cm^{-1}; black dashed line) and D_2O (1645.4 ± 0.3 and 1628.3 ± 1.9 cm^{-1}; red lines).

have shown that the vibrational frequency shifts of a localized amide I mode are dominated by the electrostatic interactions with the C═O, though there are other local modes contributing to the amide I normal mode. For simplicity, the value of the Stark tuning rate was calculated from the data assuming that the angle between the transition moment and difference dipole is 0° (note that the transition dipole has been reported to be ca. 10−20° off the C═O bond axis[68−70] and this will affect the interpretation of vibrational Stark effects for the amide I band in proteins). In support of the notion that the frequency response of this mode to an electric field is primarily due to the C═O, the observed Stark tuning rate of 1.3 cm^{-1}/(MV/cm) for both the NMA monomer in 2MeTHF and NMA-d_1 in D_2O indicates a minimal effect of N-deuteration, which was expected to alter the normal mode composition of the amide I frequency (Figure S2C−F).[68,71] The Stark spectrum of NMA in 2MeTHF (Figure S2D) indicates the presence of several C═O bands which we tentatively assign to the monomer at 1671.2 cm^{-1} and an oligomer at 1637.1 cm^{-1}, which is generally observed for NMA in low polarity organic solvents.[72] The peak at 1655 cm^{-1} is observed in both NMA and DMA, in both cases without an observable Stark feature and as such was not considered in the fitting. Furthermore, the Stark feature corresponding to the oligomeric peak is broad and of much lower intensity than the monomer (Figure S2D). This feature may arise from coupling between the NMA oligomer C═O modes,[73−76] which could lead to a breakdown in the assumptions of our Stark analysis and therefore was not characterized further. Beyond simple amides, the Stark tuning rate for the amide and β-lactam of ampicillin are significantly greater than those observed for NMA or DMA, suggesting that intramolecular H-bonding from the neighboring amine and ring strain, respectively, can have large influences on the magnitude of the Stark tuning rate.

When comparing the Stark tuning rates of the simple oxoesters, thioesters, and amides, there is a general trend that $|\Delta\vec{\mu}_{C=O}|f$ increases such that O < N < S. This indicates that the heteroatom (X) in the R−C(O)X−R moiety is the main contributor distinguishing the Stark tuning rates, with larger effects from less electronegative heteroatoms. These results suggest that there are only small differences in the linear Stark tuning rate with increasing conjugation (e.g., methyl acetate, methyl benzoate, and methyl cinnamate) and that changing the substitution (e.g., ethyl 4-aminocinnamate), ring strain (β-lactam), or intramolecular hydrogen bonding (e.g., amide mode of ampicillin) can significantly increase $|\Delta\vec{\mu}_{C=O}|f$. Furthermore, there is little to no variation in the Stark tuning rate of a given vibrational probe between different hydrogen-bonding (H-bonding) and non-hydrogen-bonding glass-forming solvents (Table 2 and Figures 1, S1, and S2). As observed with acetophenone,[3] this suggests that each carbonyl's intrinsic sensitivity to an electric field is the same in both H-bonding and non-H-bonding environments. In other words, the constant value of $|\Delta\vec{\mu}_{C=O}|f$ observed across multiple solvents suggests that both $|\Delta\vec{\mu}_{C=O}|$ and f are independent of environment.

Vibrational Solvatochromism. In order to further develop the carbonyl group as an electric field probe, we carried out vibrational solvatochromism studies on ethyl acetate, methyl benzoate, ethyl thioacetate, butyl thiobenzoate, and DMA as model compounds.

Similar to earlier work from our lab on acetophenone,[3] the C═O frequency in all solutes was observed to red-shift in solvents of increasing polarity from hexanes to aqueous solution, as shown in Figure 2. In general, the observed

DOI: 10.1021/acs.jpcb.6b08133
J. Phys. Chem. B 2016, 120, 9672−9684

solvatochromic shift in peak position between hexanes and water ($\Delta\bar{\nu} = \bar{\nu}_{hexane} - \bar{\nu}_{water}$) reflects the different magnitudes of their respective Stark tuning rates. This is evidenced by comparison of butyl thiobenzoate ($|\Delta\vec{\mu}_{C=O}|f$ = 1.37 cm^{-1}/(MV/cm)), methyl benzoate ($|\Delta\vec{\mu}_{C=O}|f$ = 1.15 cm^{-1}/(MV/cm)), and acetophenone ($|\Delta\vec{\mu}_{C=O}|f$ = 1.05 cm^{-1}/(MV/cm)),[3] which are all similarly conjugated but have decreasing solvatochromic shifts (34.0, 28.6, and 27.0 cm^{-1}, respectively) across the solvent series. However, the opposite trend is observed with respect to the Stark tuning rate for ethyl acetate and thioacetate. This may be due to the broad absorbance of the C═O peak of ethyl acetate in water, which has a prominent shoulder and complicates the analysis. This observation is consistent with studies on similar alkyl acetates where the solvents exhibit altered conformations of the terminal methyl group, resulting in differences in the *E*/*Z*-rotamer populations,[77−79] or the presence of different H-bonding configurations as observed by MD simulations and 2D IR.[80−82] Consistent with multiple H-bonding configurations, postprocessing of MD trajectories by Pazos et al. showed that the fields and frequencies of these 1- and 2-H-bonding configurations fall on the same field-frequency calibration line as other non-H-bonding solvents, consistent with a linear Stark effect.[5] For simplicity, all C═O frequencies were determined using the peak picking method and are in close agreement with those from curve-fitting except in cases where multiple peaks were observed (Table S1). Surprisingly, the solvatochromic response of the amide C═O of DMA has the largest frequency shifts of those studied (Figure 2C) of 66.9 cm^{-1}. This result is discussed further in the context of the MD simulations presented below. Consistent with previous studies,[3] we observe that there is a strong correlation between the C═O line widths, which are related to the inhomogeneous distribution of electric fields in solution, and peak positions, which are related to the average electric field experienced by the bond (Table S1).

MD Simulations and Field-Frequency Correlations. We performed molecular dynamics (MD) simulations to calculate the average solvent reaction field based on previous work by Fried et al.[3] When directly correlated to the solvatochromism measurements, this provides a calibration curve that relates the C═O frequency to the absolute electric field experienced by the carbonyl in the solvent series. Furthermore, the slope of this correlation provides a further measure of the Stark tuning rate ($|\Delta\vec{\mu}_{C=O}|$) for direct comparison to that measured by VSS ($|\Delta\vec{\mu}_{C=O}|f$) as discussed below.

Utilizing the same solvent series as the solvatochromism measurements, we have calculated the average absolute electric field experienced by the carbonyl of ethyl acetate, methyl benzoate, ethyl thioacetate, butyl thiobenzoate, and DMA. Consistent with previous studies, the average electric field (Figure 3, horizontal axis) and standard deviation (Table S1) increase with increasing solvent polarity. Additionally, for two molecules in the same solvent of similar size and conjugation, the average electric field experienced by the C═O is comparable as observed between ethyl acetate and ethyl thioacetate as well as methyl benzoate and butyl thiobenzoate. This may suggest that the solute geometry and steric considerations around the C═O are the primary determinants for the magnitude of the solvent electric field, since there are only small variations between oxoesters and thioesters of similar shape. However, for DMA, the average solvent electric field is consistently larger than that of similarly sized ethyl acetate and thioacetate, suggesting that another factor may give

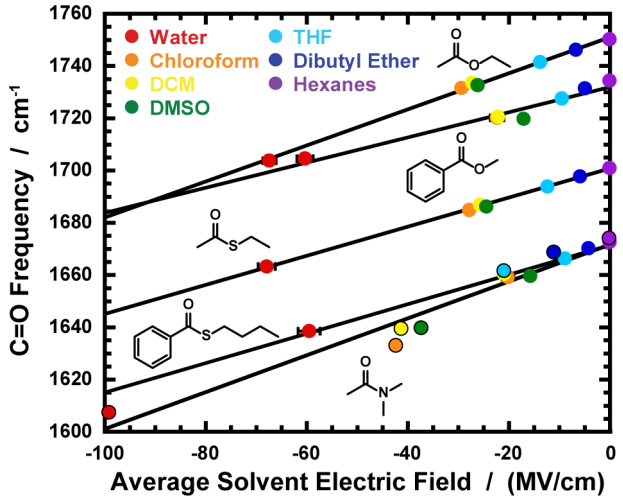

Figure 3. The sensitivity of the carbonyl stretch frequency to the electrostatic field. Plot of the C═O frequency of ethyl acetate, methyl benzoate, ethyl thioacetate, butyl thiobenzoate, and *N*,*N*-dimethylacetamide (structures shown) relative to the average calculated solvent electric field experienced by the C═O. The least-squares regression lines are $\bar{\nu}_{C=O}^{ethyl\ acetate} = 0.69|\vec{F}_{solv}| + 1751.1$ (R^2 = 0.99), $\bar{\nu}_{C=O}^{methyl\ benzoate} = 0.48|\vec{F}_{solv}| + 1732.0$ (R^2 = 0.97), $\bar{\nu}_{C=O}^{ethyl\ thioacetate} = 0.56|\vec{F}_{solv}| + 1700.8$ (R^2 = 0.99), $\bar{\nu}_{C=O}^{butyl\ thiobenzoate} = 0.56|\vec{F}_{solv}| + 1671.4$ (R^2 = 0.99), and $\bar{\nu}_{C=O}^{dimethylacetamide} = 0.70|\vec{F}_{solv}| + 1671.7$ (R^2 = 0.97), respectively. For butyl thiobenzoate in D_2O, the frequency was measured in 1:2 (% v/v) DMSO/D_2O due to low solubility and the broad feature fit to three Voigt profiles corresponding to the C═O in DMSO and aqueous environments. The C═O frequency was determined from the weighted average of the two D_2O peaks based on the integrated area from curve fitting. This peak position is in agreement with the frequency calculated from the least-squares regression line utilizing only the organic solvents (hexanes to chloroform) at 1637.3 cm^{-1} in comparison to 1638.2 cm^{-1} in 1:2 DMSO/D_2O. For clarity, the DMA data is shown in enclosed circles to distinguish between butyl thiobenzoate. Error bars on both the frequencies and electric fields are shown and may be contained within the symbols.

rise to this difference between amides and other carbonyl probes. Furthermore, these results are consistent with DMA having the largest solvatochromic frequency shifts among the probes studied, indicating that the MD simulations are able to recapitulate the trends observed by solvatochromism. While multiple peaks are occasionally observed with certain solutes and solvents, in the case of DMA, the observed shoulder at ca. 1655 cm^{-1} may be attributed to either Fermi resonances[83] (previously observed with 19-nortestosterone,[1] where shoulders appear at the same frequency across different solvents) or the noncoincidence effect,[84,85] though we observe no appreciable concentration dependence between 1 and 100 mM for the shoulder. We do not observe two separate peaks each with their own solvatochromic shifts, and the simulations exhibit single populations based on the electric field distributions. No effort was made to further deconvolve these peaks, and the major peak's center frequency was used for all field-frequency correlations, which may introduce small errors into the fits.

The linear correlation between the C═O frequency and the calculated electric field (Figure 3) is consistent with the solvent shifts being due to a linear VSE. Despite this observed linear correlation for each molecule, the slopes of the best-fit lines are not equivalent to the independently measured Stark tuning rate, and the difference is assumed to reflect subtle differences

DOI: 10.1021/acs.jpcb.6b08133
J. Phys. Chem. B 2016, 120, 9672−9684

in the magnitude of the local field factor (f). This result highlights an ongoing source of uncertainty in the analysis of solvatochromism data and its connection to VSS results (Table 1).[23] The VSS data is taken with frozen solvent glasses (to prevent solute and solvent reorientation in the applied field and dielectric breakdown), while the solvatochromism data and MD simulations apply to fluid solutions. There is no applied field in the case of solvatochromism; thus, the local field factor does not enter, whereas the VSS data is obtained in an applied electric field; hence, the data is given as $|\Delta\vec{\mu}_{C=O}|f$ in Table 1. The slope of the field-frequency correlation should equal the Stark tuning rate, $|\Delta\vec{\mu}_{C=O}|$; thus, the simplest interpretation of the variations in observed slopes (Figure 3) is that the local field correction factor is somewhat different for each compound. The observed range, f = 1.6−2.6 based on the differences in slopes of the field-frequency calibration curves ($|\Delta\vec{\mu}_{C=O}|$) relative to the experimentally measured linear Stark tuning rates ($|\Delta\vec{\mu}_{C=O}|f$; Table S2), suggests that $|\Delta\vec{\mu}_{C=O}|$ is approximately half that measured by vibrational Stark spectroscopy, that is, $f \approx 2$, consistent with earlier work and recent calculations.[1,3,53] On the other hand, there may be subtle but systematic discrepancies in the simulations of solute−solvent pairs that are not accounted for at the current level of approximation. This uncertainty makes quantitative comparison *between* probes difficult, but a single probe can be used consistently to study a system of interest using the VSE. More sophisticated treatments of the electric fields in different solvents may be possible;[9] however, these treatments involve large numbers of parameters and likely would not affect the main conclusions on the magnitude of the electric field, as the carbonyl response to different environments has been shown to be dominated by electrostatic interactions.[9,86−90]

Summary. In order to further utilize carbonyl vibrational probes and interpret frequency shifts in terms of electric fields in condensed matter, we have measured the Stark tuning rate of oxoesters, thioesters, and amides through vibrational Stark spectroscopy and vibrational solvatochromism correlated with MD simulations. These findings further indicate that the frequency response of the C═O stretch is primarily electrostatic in nature, as indicated by the linear field-frequency calibration and the consistency of the measured Stark tuning rates in both H-bonding and non-H-bonding frozen glasses. Therefore, the C═O vibrational probe is well suited to interrogate diverse molecular interactions such as catalysis and binding using the vibrational Stark effect, as exemplified in the following section, where we have selected representative examples from Table 1.

B. Applications to Probes at Enzyme Active Sites. The framework used to apply VSE probes to parse the electrostatic contribution to catalysis is shown in a simplified reaction coordinate diagram in Figure 4 for some of the major classes of carbonyl chemical reactions found in enzymes. Within this framework, we are specifically focusing on the degree to which the transition state is stabilized by interaction with the total field, $\vec{F}_{enz}$, from the surrounding protein. This includes very local interactions such as specific hydrogen bonds but also more global contributions that are less easily visualized (these effects need not work in concert). For simplicity, we show the bond(s) involved in the substrate as having a small dipole moment, $\vec{\mu}_{GS}$ (often not the case), with a substantial increase in the dipole moment of the transition state (e.g., $|\vec{\mu}_{TS}| > |\vec{\mu}_{GS}|$, a common situation) associated with the reaction, and $\Delta\vec{\mu}_{rxn} \equiv \vec{\mu}_{TS} - \vec{\mu}_{GS}$. The effect of the protein field on the free energy of activation is then given by

$$\Delta\Delta G^{\ddagger} = -\vec{F}_{enz}\cdot\Delta\vec{\mu}_{rxn} \quad (2)$$

Note that the effect of $\vec{F}_{enz}$ is illustrated in Figure 4 as stabilizing the transition state, but this depends on the relative orientation of $\vec{F}_{enz}$ and $\Delta\vec{\mu}_{rxn}$. By placing a calibrated vibrational probe that closely mimics the presumed transition state into the enzyme active site, as close as possible to the bond experiencing $\Delta\vec{\mu}_{rxn}$, the observed frequency shifts detected by IR or Raman spectroscopy for a series of variants whose free energies of activation have been measured separately can provide information on the relationship, if any, between the free energy of activation and the protein field. As shown in part A, the frequency response of carbonyl vibrational probes can be explained entirely using the linear VSE, providing a means for quantifying the catalytically relevant electric fields in reactions in which the rate-determining step involves charge rearrangements occurring at the carbonyl, assuming that the probe is oriented such that it experiences some projection of the relevant active site electric field. While chemical positioning and distal binding interactions with the substrate may be relevant for catalysis, these effects are not part of electric field catalysis and cannot be explored using the VSE method.[1,91] This strategy has been described earlier for KSI,[1,49] and in the following, we use this framework and the results from part A to reinterpret IR and Raman data already in the literature for several enzymes. Note that, while a relationship between the free energy and protein field may have significance, a large electric field, in and of itself, is not necessarily indicative of a good catalyst. As extensively discussed elsewhere,[91−96] water (where the "mechanism-filtered" reference reaction takes place) is a poor catalyst, though it has a large electric field, for reactions which involve large changes in the magnitude and/or reorientation of the dipoles over the reaction coordinate.

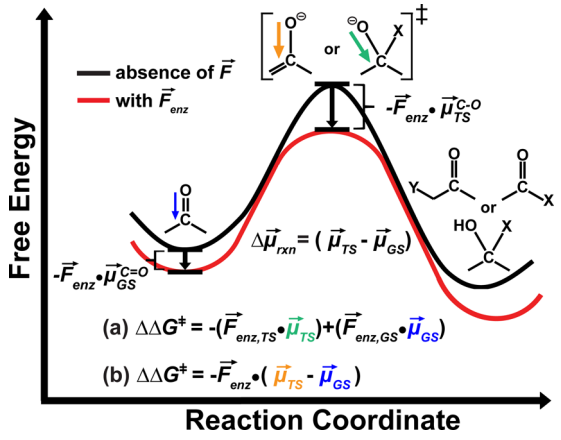

Figure 4. The role of an electric field on catalysis. The reaction coordinate diagram for how an electric field can facilitate an increase in catalytic rate through transition state stabilization as governed by the enzyme field ($\vec{F}_{enz}$) and the reaction difference dipole ($\Delta\vec{\mu}_{rxn}$). Two cases of electric field catalysis are illustrated, (a) one in which the ground state (GS) and transition state (TS) dipole reorient over the course of the reaction (e.g., the tetrahedral TS) and the other is the simpler case (b) where the magnitude of the dipole only increases but does not change direction (e.g., the enolate TS).

Dehalogenase. 4-Chlorobenzoyl-CoA dehalogenase (Dehalogenase) is a member of the Crotonase superfamily, which possesses common structural and catalytic features to stabilize

DOI: 10.1021/acs.jpcb.6b08133
J. Phys. Chem. B 2016, 120, 9672−9684

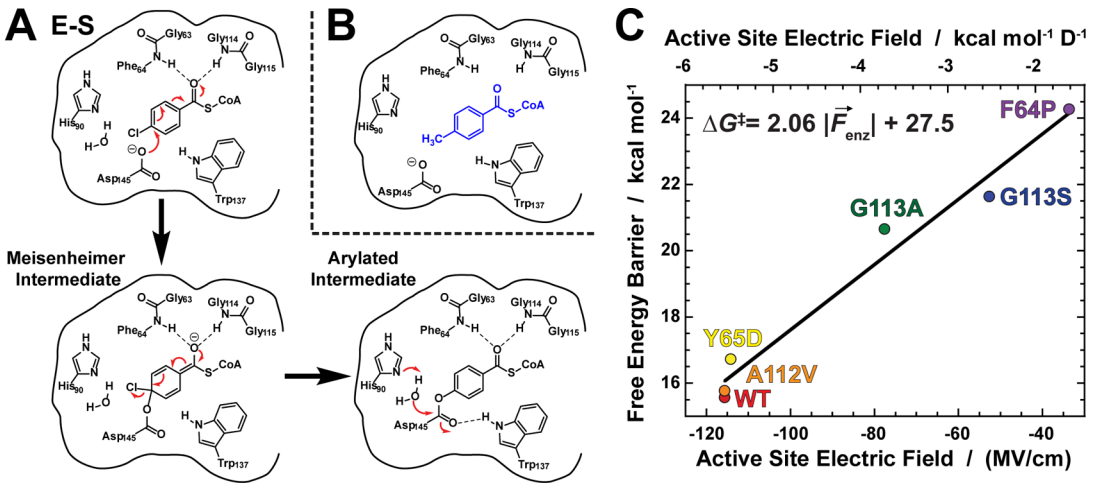

Figure 5. Vibrational Stark effects and electric fields at the active site of 4-chlorobenzoyl-CoA dehalogenase. (A) The chemical mechanism of the reaction catalyzed by Dehalogenase through the arylated intermediate as adapted from Clarkson et al. and PDB 1NZY.[46] The aryl-intermediate proceeds to be hydrolyzed by the active site water followed by product release (not shown). (B) The complex between Dehalogenase and the substrate analogue, 4-methylbenzoyl-CoA, used by Dong et al. to obtain C═O Raman data at the active site.[45] (C) Plot of the measured free energy of activation for a series of mutants relative to the active site electric field. Carbonyl frequencies and single-turnover rates for the mutant series as reported by Dong et al.[45] WT: 1612 cm^{-1}, k_{obs} = 24 s^{-1}, A112V: 1612 cm^{-1}, k_{obs} = 17 s^{-1}, Y65D: 1613 cm^{-1}, k_{obs} = 3.4 s^{-1}, G113A: 1638 cm^{-1}, k_{obs} = 4.5 × 10^{-3} s^{-1}, G113S: 1655 cm^{-1}, k_{obs} = 8.5 × 10^{-4} s^{-1}, F64P: 1668 cm^{-1}, k_{obs} = 1 × 10^{-5} s^{-1}. A linear relationship is observed between the free energy barrier ($\Delta G^{\ddagger}$) and the active site electric field based on the VSE analysis. The least-squares regression line $\Delta G^{\ddagger} = 2.06|\vec{F}_{enz}| + 27.5$ (R^2 = 0.97) is reported in kcal mol^{-1}, where the slope is in units of Debye (D) and $|\vec{F}_{enz}|$ is in MV/cm or kcal mol^{-1} D^{-1} (upper *x*-axis).

enolate intermediates in the oxyanion hole.[97] Dehalogenase catalyzes the hydrolytic dehalogenation of 4-chlorobenzoyl-CoA to 4-hydroxybenzoyl-CoA through a stepwise reaction mechanism that proceeds from the initial addition of Asp145 to the C4 position of the benzoyl ring, forming the Meisenheimer intermediate, followed by removal of the chloride ion and subsequent hydrolysis of the arylated enzyme (Figure 5A).[45] This enzyme is proposed to be a recent evolutionary response to increased synthetic chlorinated organic pollutants in the environment as part of the 4-chlorobenzoate degradation pathway in *Pseudomonas* species CBS3.[98]

Using Raman spectroscopy, Dong et al.[45] observed that there is a linear relationship between the single-turnover rate (k_{obs}), where the formation of the Meisenheimer intermediate is assumed to be rate-limiting, and the thioester C═O vibrational frequency using both the natural substrate and inhibitors for a series of mutants.[45] The rate changes by 2.4 × 10^6 and the frequency varies by 61 cm^{-1} across the mutant series, clearly suggesting a role for electrostatics, but there was no way to go beyond an empirical description correlating frequency shifts with hydrogen-bonding strength.[45,46]

Assuming that the Stark tuning rate of the Dehalogenase inhibitor, 4-methylbenzoyl-CoA (Figure 5B), has a similar Stark tuning rate as that of butyl thiobenzoate, $|\Delta\vec{\mu}_{C=O}|f \sim 1.37$ cm^{-1}/(MV/cm) (Table 1), we can interpret these frequency shifts in terms of electric fields (Figure 5C). This analysis relies on the following: the field-frequency relationship of butyl thiobenzoate ($f \approx 2$) is a reasonable estimate for the inhibitor, the calculated electric field of ethyl 4-methylthiobenzoate in water is −58.5 MV/cm, and the known frequency of the C═O stretch of 4-methylbenzoyl-CoA in water is 1651 cm^{-1}.[46] Plotted in Figure 5C are the free energies of activation obtained by Dong et al. on the *y*-axis and their observed Raman frequencies,[45] converted into electric fields through the combination of VSS, solvatochromism, and MD simulations on the *x*-axis. These data fit very well to a line, where $\Delta G^{\ddagger} = 2.06\vec{F}_{enz} + 27.5$. The slope of the least-squares regression line, 2.06 D (see units on the upper *x*-axis), is the reaction difference dipole, $\Delta\vec{\mu}_{rxn}$, which is a measure of the change in charge distribution between the ground and transition states. This value is about twice as large as that observed for KSI,[1] as may be expected given the larger charge rearrangement between the ground state and Meisenheimer intermediate. The intercept at 27.5 kcal mol^{-1} corresponds to the hypothetical free energy barrier if Dehalogenase did not exert any stabilizing electric field, i.e., $\vec{F}_{enz}$ = 0, suggesting that 11.9 kcal mol^{-1} of the enzyme's catalytic power comes from a large stabilizing electric field, a rate enhancement of $10^{8.7}$-fold relative to the reaction in the absence of an electric field. As noted previously,[1] rescaling of the calculated electric fields (e.g., due to the local field factor) will not affect the primary finding that the active site electric field is directly correlated with lowering the activation barrier, though it will affect the magnitude of $\Delta\vec{\mu}_{rxn}$. To our knowledge, the enthalpy of activation has not been measured for the wild-type enzyme, though the intercept is in close agreement with the calculated enthalpic contribution to catalysis of $\Delta H^{\ddagger}$ = 27.4 kcal mol^{-1} for the nucleophilic aromatic substitution reaction in aqueous solution.[99] Furthermore, on the basis of the predicted uncatalyzed rate in solution of 2.3 × 10^{-15} s^{-1},[99] it is estimated that approximately 55% of the rate enhancement comes from the presence of a large electric field at the C═O bond. The remaining significant portion of the enzyme's rate enhancement can be attributed to other factors, largely entropic, based on the predicted rate in solution. There is likely a significant contribution from chemical positioning (entropic) of Asp145 and the active site water necessary for formation of the Meisenheimer intermediate and subsequent hydrolysis.

Although Dehalogenase has only a modest catalytic rate and a smaller active site electric field compared with KSI, a larger $\Delta\vec{\mu}_{rxn}$ allows for a greater overall rate enhancement due to electric field catalysis (as seen in Figure 4, the effect scales linearly with $\Delta\vec{\mu}_{rxn}$ and $\vec{F}_{enz}$). In other words, proteins that catalyze reactions with larger reaction difference dipoles can

DOI: 10.1021/acs.jpcb.6b08133
J. Phys. Chem. B 2016, 120, 9672−9684

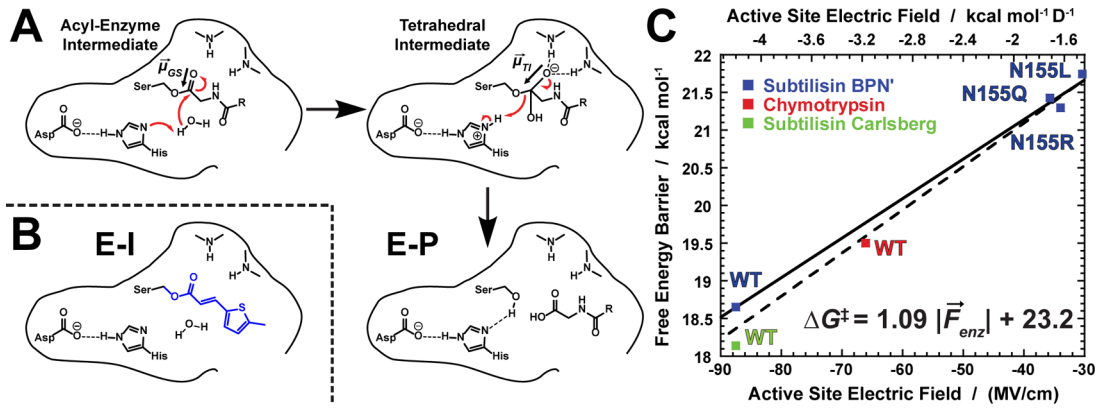

Figure 6. Vibrational Stark effects in the active site of serine proteases. (A) General mechanism for serine proteases beginning from the acyl-intermediate with rate-limiting hydrolysis and deacylation. The ground state ($\vec{\mu}_{GS}$) and tetrahedral intermediate ($\vec{\mu}_{TI}$) dipoles are illustrated with respect to the oxyanion hole. (B) The covalent acylation intermediate formed from (5-methylthienyl)acryloyl as employed by Tonge et al. for resonance Raman studies.[29] (C) The linear correlation between the free energy barrier and active site electric field as experienced by the ground state acyl-intermediate. The frequencies and deacylation rates as reported by Tonge et al. are as follows:[29] WT BPN′ 1673 cm^{-1}, k_3 = 0.13 s^{-1}, N155R 1702 cm^{-1}, k_3 = 0.0012 s^{-1}, N155Q 1703 cm^{-1}, k_3 = 0.0015 s^{-1}, N155L 1705 cm^{-1}, k_3 = 0.0007 s^{-1}, WT Chymotrypsin 1685 cm^{-1}, k_3 = 0.031 s^{-1}, WT Carlsberg 1673 cm^{-1}, k_3 = 0.31 s^{-1}. The least-squares regression line for Subtilisin BPN′ and mutants (blue) is $\Delta G^{\ddagger} = 1.09|\vec{F}_{enz}| + 23.2$ (R^2 = 0.99), where $|\vec{F}_{enz}|$ is reported in units of kcal mol^{-1} D^{-1} (upper axis) and the slope is in Debye. The dashed line is a fit to all serine proteases with 5-MeTA and least-squares regression line of $\Delta G^{\ddagger} = 1.20|\vec{F}_{enz}| + 23.4$ (R^2 = 0.98).

achieve the same catalytic rate enhancement with smaller active site electric fields, a concept we have termed the "*catalyzability*" of the reaction;[91] this likely has important implications in protein evolution and catalyst design, and Dehalogenase would be a good target.

Serine Proteases. Serine proteases have been extensively studied, often highlighting the importance of a preorganized active site on catalytic function.[100−102] The reaction mechanism is illustrated in Figure 6A and showcases the catalytic triad which participates in peptide bond hydrolysis leading to the acyl-intermediate. The acyl-intermediate is then attacked by an activated water molecule during the rate-limiting step to form the anionic tetrahedral transition state, which proceeds to form the hydrolyzed product. Despite much study, there has been continuing debate on the molecular origins of the catalytic power in serine proteases, either from low-barrier hydrogen bonds (LBHBs) in the catalytic triad (e.g., Ser-His-Asp as observed in chymotrypsin) and/or transition state stabilization from the oxyanion hole.[100,101,103]

In an effort to elucidate the physical origins of catalysis in serine proteases, Tonge et al.[29] utilized resonance Raman spectroscopy to study the frequency shifts of acyl-intermediates of Chymotrypsin, Subtilisin BPN′, and Subtilisin Carlsberg. Using 5-methylthienyl acrylate (5-MeTA), these authors observed that there was a linear relationship between the C═O frequency of the acyl-intermediate (Figure 6B) and the rate-limiting deacylation kinetics (k_3).[29] In order to rationalize this result, vibrational solvatochromism was employed along with empirical correlations to relate these frequency shifts to changes in hydrogen-bonding strength and C═O bond length in the active site. Note that it is common to relate red shifts with changes in bond length and double bond character, i.e., to a change in the force constant for the oscillator (often called "bond polarization"). However, we have shown in earlier work[1,3,23] and for the compounds discussed here that these frequency shifts can be entirely accounted for by changes in the electric field exerted by different solvents as they interact with the solute oscillator; this treatment explicitly does not alter the physical properties of the solutes, and a recent theoretical analysis by List et al.[7] is consistent with this assumption. Note also that solvent dielectric constant, while convenient and widely used as a description of bulk solvent properties, does not provide a molecular picture and has no units, in contrast to the electric field.

Solvatochromic measurements with the methyl ester of 5-MeTA showed that the C═O frequency shifts by 36 cm^{-1} from hexanes to water.[37] A similar solvatochromic shift of ca. 38 cm^{-1} was observed with methyl cinnamate in the same solvent series (Figure S3). Additionally, the calculated electric fields of methyl cinnamate and 5-MeTA in water are 60.3 ± 1.9 and 58.1 ± 1.3 MV/cm, respectively, in agreement with the observation in part A that two molecules of similar size and conjugation will experience electric fields of the same magnitude. On the basis of these results, it can be reasonably assumed that the Stark tuning rate of 5-MeTA is approximately that of methyl cinnamate ($|\Delta\vec{\mu}_{C=O}|f$ = 1.12 cm^{-1}/(MV/cm) and f = 2), and we use this value to reinterpret these findings in terms of the VSE.

As with KSI and Dehalogenase, the Stark tuning rate, frequency-field calibration combined with solvatochromism, Raman and rate data from Tonge et al.[29,37] allow for quantification of the electric fields experienced by the acyl-intermediate in the protein active site, as shown in Figure 6C. The intercept of the least-squares regression line is 23.2 kcal mol^{-1} and represents the projection onto the probe transition dipole (approximately parallel to the probe bond axis) in the inhibitor used to collect the Raman data. Because of the geometry change going to the transition state, this projection is a lower limit to the hypothetical free energy barrier if these proteases possessed no stabilizing electric field, a shortcoming that is discussed below. The slope, which gives an estimate for $|\Delta\vec{\mu}_{rxn}|$ of 1.09 D, is comparable to that observed in KSI. We can also add data for similar measurements made with 5-MeTA in α-Chymotrypsin and Subtilisin Carlsberg which catalyze the same reaction via a shared mechanism. As seen in Figure 6C, dotted line, these data lie on essentially the same least-squares regression line as that of the Subtilisin BPN′ series, suggesting

DOI: 10.1021/acs.jpcb.6b08133
J. Phys. Chem. B 2016, 120, 9672−9684

that $|\Delta\vec{\mu}_{rxn}|$ is an intrinsic property of the reaction rather than enzyme-dependent.

In contrast to the inhibitors used to probe KSI and Dehalogenase, whose ground-state and transition-state C−O geometries are expected to be very similar, this will not be true for serine proteases and many other enzymes that proceed through tetrahedral transition states. A change in the orientation between $\vec{\mu}_{TS}$ and $\vec{\mu}_{GS}$ means that the electric field experienced in the two states could be significantly different. On the basis of the model in Figure 4, an enzyme can achieve the greatest rate enhancement by maximizing the transition state and minimizing the ground-state electric fields, which will reflect the preorganization of the protein (Figure S4). Enzymes that can utilize these geometry changes to preferentially stabilize or anticipate the transition state would be able to achieve larger rate enhancements by electric field catalysis.[91] However, the experiment reports on the projection of the electric field on the ground state C═O bond, which is not necessarily the orientation with the maximum electric field. Therefore, the extent to which catalytic information can be parsed from the VSE measurements is limited by the availability of probes that bind in an orientation resembling the transition state. While there are single bond transition state analogues for proteases, these probes would have frequencies in a more cluttered region of the infrared and, by virtue of being low-frequency single bond modes, they may exhibit increased mode-mixing in the normal modes and nonlinear Stark effects.

On the basis of this discussion, the analysis likely provides a lower limit for the actual magnitude of the electric field and its role in catalysis. Furthermore, the apparent $\Delta\vec{\mu}_{rxn}$ as shown in Figure 6C is actually a measure of the change in the free energy barrier as a function of the change in electric field experienced by the C═O probe across a series of mutants ($\Delta\Delta G^{\ddagger}/\Delta\vec{F}^{C=O}_{enz}$) and may be expected to differ for a transition state analogue. There is experimental evidence for this notion in the literature. Doran et al.[44] observed a negative linear correlation between the C═O frequency of the acyl-intermediate and catalytic rate in several cysteine proteases, in contrast to all previously observed frequency-rate correlations. While this was previously rationalized on the basis of changes in polarization or resonance forms in the active site,[44] in the context of VSE, we can interpret this result to suggest that the active site electric field has evolved to minimize the ground state electric field and increase the catalytic advantage from transition state stabilization expected from a preorganized enzyme active site (for further discussion, see Figure S4). It is worth noting that these observed fields are still stabilizing the ground state C═O, since $\vec{F}^{C=O}_{enz} < 0$, and cannot be taken as an example of ground state destabilization based on the VSE model and in agreement with Warshel et al.[94] Although untested, this may suggest that the electric field varies to a greater extent in cysteine versus serine proteases over the angle displacement between the ground state (C═O) and transition state (C—O$^-$) bond axes. Though we hypothesize that the fields experienced in the transition state would be significantly greater than those observed for the acyl-intermediate, the current analysis clearly indicates a significant role for electric fields in catalysis. These differences in the electric field in the transition versus ground state would reflect the preorganization of these proteases, suggesting a role for these electric fields to guide enzyme evolution and protein design.

CONCLUSIONS

KSI is the most extensively studied enzyme using vibrational Stark effects,[1,49] but many other examples can be described within the same framework. The generalizability of the VSE model provides a quantitative framework for discussing and interpreting vibrational frequency shifts in terms of electric fields. The characterization of oxoester, thioester, and amide model compounds expands upon the available carbonyl vibrational probes that can be used for exploring electric fields. Through the combined methods of vibrational Stark spectroscopy, vibrational solvatochromism, and MD simulations, these carbonyl probes all exhibit a linear field-frequency relationship and constant Stark tuning rate across multiple environments, suggesting that the response to an electric field is primarily due to the linear Stark effect.

These findings enable a more comprehensive method for rationalizing noncovalent interactions in many enzymatic systems, as illustrated in part B, which illustrates the role of electric fields to facilitate catalysis. Measurement of VSEs in proteins and other systems provides a method for relating frequency shifts to electric fields, a general physical quantity, which may have significant applications in catalyst design.

ASSOCIATED CONTENT

Supporting Information

The Supporting Information is available free of charge on the ACS Publications website at DOI: 10.1021/acs.jpcb.6b08133.

Additional vibrational Stark spectrum of oxoesters and amides, IR solvatochromism of methyl *trans*-cinnamate, discussion of the relation between the reaction coordinate geometry and the active site electric field, tabulated frequencies, fwhm, and electric fields from solvatochromism and MD simulations, and comparison of the Stark tuning rates from VSS and field-frequency correlations (PDF)

AUTHOR INFORMATION

Notes

The authors declare no competing financial interest.

ACKNOWLEDGMENTS

The authors would like to thank Dr. Stephen Fried and Yufan Wu for helpful discussions on methods, results, and interpretations. This work was supported in part by grants from the NIH (Grant GM27738 and GM118044).

REFERENCES

(1) Fried, S. D.; Bagchi, S.; Boxer, S. G. Extreme Electric Fields Power Catalysis in the Active Site of Ketosteroid Isomerase. *Science* **2014**, *346*, 1510−1514.

(2) Andrews, S. S.; Boxer, S. G. Vibrational Stark Effects of Nitriles I. Methods and Experimental Results. *J. Phys. Chem. A* **2000**, *104*, 11853−11863.

(3) Fried, S. D.; Bagchi, S.; Boxer, S. G. Measuring Electrostatic Fields in Both Hydrogen-Bonding and Non-Hydrogen-Bonding Environments Using Carbonyl Vibrational Probes. *J. Am. Chem. Soc.* **2013**, *135*, 11181−11192.

(4) Fried, S. D.; Wang, L. P.; Boxer, S. G.; Ren, P.; Pande, V. S. Calculations of the Electric Fields in Liquid Solutions. *J. Phys. Chem. B* **2013**, *117*, 16236−16248.

(5) Pazos, I. M.; Ghosh, A.; Tucker, M. J.; Gai, F. Ester Carbonyl Vibration as a Sensitive Probe of Protein Local Electric Field. *Angew. Chem., Int. Ed.* **2014**, *53*, 6080−6084.

DOI: 10.1021/acs.jpcb.6b08133
J. Phys. Chem. B 2016, 120, 9672−9684

(6) Reimers, J. R.; Hush, N. S. Vibrational Stark Spectroscopy 3. Accurate Benchmark Ab Initio and Density Functional Calculations for CO and CN-. *J. Phys. Chem. A* **1999**, *103*, 10580−10587.
(7) List, N. H.; Beerepoot, M. T.; Olsen, J. M.; Gao, B.; Ruud, K.; Jensen, H. J.; Kongsted, J. Molecular Quantum Mechanical Gradients within the Polarizable Embedding Approach—Application to the Internal Vibrational Stark Shift of Acetophenone. *J. Chem. Phys.* **2015**, *142*, 034119.
(8) Choi, J.-H.; Cho, M. Vibrational Solvatochromism and Electrochromism of Infrared Probe Molecules Containing C≡O, C≡N, C═O, or C-F Vibrational Chromophore. *J. Chem. Phys.* **2011**, *134*, 154513.
(9) Błasiak, B.; Cho, M. Vibrational Solvatochromism. III. Rigorous Treatment of the Dispersion Interaction Contribution. *J. Chem. Phys.* **2015**, *143*, 164111.
(10) Sen, S.; Boda, M.; Lata, S. V.; Naresh, G. N. Internal Electric Fields in Small Water Clusters $[(H_2O)_n$; n = 2−6]. *Phys. Chem. Chem. Phys.* **2016**, *18*, 16730−16737.
(11) Fafarman, A. T.; Sigala, P. A.; Schwans, J. P.; Fenn, T. D.; Herschlag, D.; Boxer, S. G. Quantitative, Directional Measurement of Electric Field Heterogeneity in the Active Site of Ketosteroid Isomerase. *Proc. Natl. Acad. Sci. U. S. A.* **2012**, *109*, E299−308.
(12) Kim, H.; Cho, M. Infrared Probes for Studying the Structure and Dynamics of Biomolecules. *Chem. Rev.* **2013**, *113*, 5817−5847.
(13) Liu, C. T.; Layfield, J. P.; Stewart, R. J., III; French, J. B.; Hanoian, P.; Asbury, J. B.; Hammes-Schiffer, S.; Benkovic, S. J. Probing the Electrostatics of Active Site Microenvironments Along the Catalytic Cycle for *Escherichia coli* Dihydrofolate Reductase. *J. Am. Chem. Soc.* **2014**, *136*, 10349−10360.
(14) Bazewicz, C. G.; Lipkin, J. S.; Smith, E. E.; Liskov, M. T.; Brewer, S. H. Expanding the Utility of 4-Cyano-L-Phenylalanine as a Vibrational Reporter of Protein Environments. *J. Phys. Chem. B* **2012**, *116*, 10824−10831.
(15) Levinson, N. M.; Boxer, S. G. A Conserved Water-Mediated Hydrogen Bond Network Defines Bosutinib's Kinase Selectivity. *Nat. Chem. Biol.* **2014**, *10*, 127−132.
(16) Bagchi, S.; Fried, S. D.; Boxer, S. G. A Solvatochromic Model Calibrates Nitriles' Vibrational Frequencies to Electrostatic Fields. *J. Am. Chem. Soc.* **2012**, *134*, 10373−10376.
(17) Aschaffenburg, D. J.; Moog, R. S. Probing Hydrogen Bonding Environments: Solvatochromic Effects on the CN Vibration of Benzonitrile. *J. Phys. Chem. B* **2009**, *113*, 12736−12743.
(18) Choi, J.-H.; Oh, K.-I.; Lee, H.; Lee, C.; Cho, M. Nitrile and Thiocyanate IR Probes: Quantum Chemistry Calculation Studies and Multivariate Least-Square Fitting Analysis. *J. Chem. Phys.* **2008**, *128*, 134506.
(19) Deb, P.; Haldar, T.; Kashid, S. M.; Banerjee, S.; Chakrabarty, S.; Bagchi, S. Correlating Nitrile IR Frequencies to Local Electrostatics Quantifies Noncovalent Interactions of Peptides and Proteins. *J. Phys. Chem. B* **2016**, *120*, 4034−4046.
(20) Kashid, S. M.; Bagchi, S. Experimental Determination of the Electrostatic Nature of Carbonyl Hydrogen-Bonding Interactions Using IR-NMR Correlations. *J. Phys. Chem. Lett.* **2014**, *5*, 3211−3215.
(21) Park, E. S.; Andrews, S. S.; Hu, R. B.; Boxer, S. G. Vibrational Stark Spectroscopy in Proteins: A Probe and Calibration for Electrostatic Fields. *J. Phys. Chem. B* **1999**, *103*, 9813−9817.
(22) Park, E. S.; Boxer, S. G. Origins of the Sensitivity of Molecular Vibrations to Electric Fields: Carbonyl and Nitrosyl Stretches in Model Compounds and Proteins. *J. Phys. Chem. B* **2002**, *106*, 5800−5806.
(23) Fried, S. D.; Boxer, S. G. Measuring Electric Fields and Noncovalent Interactions Using the Vibrational Stark Effect. *Acc. Chem. Res.* **2015**, *48*, 998−1006.
(24) Taylor, K. L.; Liu, R.-Q.; Liang, P.-H.; Price, J.; Dunaway-Mariano, D.; Tonge, P. J.; Clarkson, J.; Carey, P. R. Evidence for Electrophilic Catalysis in the 4-Chlorobenzoyl-CoA Dehalogenase Reaction: UV, Raman, and ^{13}C-NMR Spectral Studies of Dehalogenase Complexes of Benzoyl-CoA Adducts. *Biochemistry* **1995**, *34*, 13881−13888.
(25) Carey, P. R. Spectroscopic Characterization of Distortion in Enzyme Complexes. *Chem. Rev.* **2006**, *106*, 3043−3054.
(26) Belasco, J. G.; Knowles, J. R. Direct Observation of Substrate Distortion by Triosephosphate Isomerase Using Fourier Transform Infrared Spectroscopy. *Biochemistry* **1980**, *19*, 472−477.
(27) Belasco, J. G.; Knowles, J. R. Polarization of Substrate Carbonyl Groups by Yeast Aldolase: Investigation by Fourier Transform Infrared Spectroscopy. *Biochemistry* **1983**, *22*, 122−129.
(28) Kurz, L. C.; Drysdale, G. R. Evidence from Fourier Transform Infrared Spectroscopy for Polarization of the Carbonyl of Oxaloacetate in the Active Site of Citrate Synthase. *Biochemistry* **1987**, *26*, 2623−2627.
(29) Tonge, P. J.; Carey, P. R. Length of the Acyl Carbonyl Bond in Acyl-Serine Proteases Correlates with Reactivity. *Biochemistry* **1990**, *29*, 10723−10727.
(30) Peng, H.-L.; Deng, H.; Dyer, R. B.; Callender, R. Energy Landscape of the Michaelis Complex of Lactate Dehydrogenase: Relationship to Catalytic Mechanism. *Biochemistry* **2014**, *53*, 1849−1857.
(31) Anderson, V. E. Quantifying Energetic Contributions to Ground State Destabilization. *Arch. Biochem. Biophys.* **2005**, *433*, 27−33.
(32) Hokenson, M. J.; Cope, G. A.; Lewis, E. R.; Oberg, K. A.; Fink, A. L. Enzyme-Induced Strain/Distortion in the Ground-State ES Complex in β-Lactamase Catalysis Revealed by FTIR. *Biochemistry* **2000**, *39*, 6538−6545.
(33) Fisher, J.; Belasco, J. G.; Khosla, S.; Knowles, J. R. β-Lactamase Proceeds via an Acyl-Enzyme Intermediate. Interaction of *Escherichia coli* RTEM Enzyme with Cefoxitin. *Biochemistry* **1980**, *19*, 2895−2901.
(34) Wilkinson, A.-S.; Ward, S.; Kania, M.; Page, M. G. P.; Wharton, C. W. Multiple Conformations of the Acylenzyme Formed in the Hydrolysis of Methicillin by *Citrobacter freundii* β-Lactamase: a Time-Resolved FTIR Spectroscopic Study. *Biochemistry* **1999**, *38*, 3851−3856.
(35) Wilkinson, A.-S.; Bryant, P. K.; Meroueh, S. O.; Page, M. G. P.; Mobashery, S.; Wharton, C. W. A Dynamic Structure for the Acyl-Enzyme Species of the Antibiotic Aztreonam with the *Citrobacter freundii* β-Lactamase Revealed by Infrared Spectroscopy and Molecular Dynamics Simulations. *Biochemistry* **2003**, *42*, 1950−1957.
(36) Chen, D.; Yue, K. T.; Martin, C.; Rhee, K. W.; Sloan, D.; Callender, R. Classical Raman Spectroscopic Studies of NADH and NAD^+ Bound to Liver Alcohol Dehydrogenase by Difference Techniques. *Biochemistry* **1987**, *26*, 4776−4784.
(37) Tonge, P. J.; Carey, P. R. Direct Observation of the Titration of Substrate Carbonyl Groups in the Active Site of α-Chymotrypsin by Resonance Raman Spectroscopy. *Biochemistry* **1989**, *28*, 6701−6709.
(38) Tonge, P. J.; Pusztai, M.; White, A. J.; Wharton, C. W.; Carey, P. R. Resonance Raman and Fourier Transform Infrared Spectroscopic Studies of the Acyl Carbonyl Group in [3-(5-Methyl-2-thienyl)-acryloyl]chymotrypsin: Evidence for Artifacts in the Spectra Obtained by Both Techniques. *Biochemistry* **1991**, *30*, 4790−4795.
(39) White, A. J.; Wharton, C. W. Hydrogen-Bonding in Enzyme Catalysis. Fourier-Transform Infrared Detection of Ground-State Electronic Strain in Acyl-Chymotrypsins and Analysis of the Kinetic Consequences. *Biochem. J.* **1990**, *270*, 627−637.
(40) White, A. J.; Drabble, K.; Ward, S.; Wharton, C. W. Analysis and Elimination of Protein Perturbation in Infrared Difference Spectra of Acyl-Chymotrypsin Ester Carbonyl Groups by Using ^{13}C Isotopic Substitution. *Biochem. J.* **1992**, *287*, 317−323.
(41) Gray, J. V.; Knowles, J. R. Monofunctional Chorismate Mutase from *Bacillus subtilis*: FTIR Studies and the Mechanism of Action of the Enzyme. *Biochemistry* **1994**, *33*, 9953−9959.
(42) Deng, H.; Zheng, J.; Clarke, A.; Holbrook, J. J.; Callender, R.; Burgner, J. W. Source of Catalysis in the Lactate Dehydrogenase System. Ground-State Interactions in the Enzyme•Substrate Complex. *Biochemistry* **1994**, *33*, 2297−2305.
(43) D'Ordine, R. L.; Tonge, P. J.; Carey, P. R.; Anderson, V. E. Electronic Rearrangement Induced by Substrate Analog Binding to the Enoyl-CoA Hydratase Active Site: Evidence for Substrate Activation. *Biochemistry* **1994**, *33*, 12635−12643.

DOI: 10.1021/acs.jpcb.6b08133
J. Phys. Chem. B 2016, 120, 9672−9684

(44) Doran, J. D.; Carey, P. R. α-Helix Dipoles and Catalysis: Absorption and Raman Spectroscopic Studies of Acyl Cysteine Proteases. *Biochemistry* **1996**, *35*, 12495−12502.
(45) Dong, J.; Lu, X.; Wei, Y.; Luo, L.; Dunaway-Mariano, D.; Carey, P. R. The Strength of Dehalogenase-Substrate Hydrogen Bonding Correlates with the Rate of Meisenheimer Intermediate Formation. *Biochemistry* **2003**, *42*, 9482−9490.
(46) Clarkson, J.; Tonge, P. J.; Taylor, K. L.; Dunaway-Mariano, D.; Carey, P. R. Raman Study of the Polarizing Forces Promoting Catalysis in 4-Chlorobenzoate-CoA Dehalogenase. *Biochemistry* **1997**, *36*, 10192−10199.
(47) Chittock, R. S.; Ward, S.; Wilkinson, A.-S.; Caspers, P.; Mensch, B.; Page, M. G. P.; Wharton, C. W. Hydrogen Bonding and Protein Perturbation in β-Lactam Acyl-Enzymes of *Streptococcus pneumoniae* Penicillin-Binding Protein PBP2x. *Biochem. J.* **1999**, *338*, 153−159.
(48) Dong, J.; Drohat, A. C.; Stivers, J. T.; Pankiewicz, K. W.; Carey, P. R. Raman Spectroscopy of Uracil DNA Glycosylase-DNA Complexes: Insights into DNA Damage Recognition and Catalysis. *Biochemistry* **2000**, *39*, 13241−13250.
(49) Wu, Y.; Boxer, S. G. A Critical Test of the Electrostatic Contribution to Catalysis with Non-Canonical Amino Acids in Ketosteroid Isomerase. *J. Am. Chem. Soc.* **2016**, DOI: 10.1021/jacs.6b06843.
(50) Suydam, I. T.; Boxer, S. G. Vibrational Stark Effects Calibrate the Sensitivity of Vibrational Probes for Electric Fields in Proteins. *Biochemistry* **2003**, *42*, 12050−12055.
(51) Andrews, S. S.; Boxer, S. G. A Liquid Nitrogen Immersion Cryostat for Optical Measurements. *Rev. Sci. Instrum.* **2000**, *71*, 3567−3569.
(52) Bublitz, G. U.; Boxer, S. G. Stark Spectroscopy: Applications in Chemistry, Biology, and Materials Science. *Annu. Rev. Phys. Chem.* **1997**, *48*, 213−242.
(53) Davari, N.; Daub, C. D.; Åstrand, P.-O.; Unge, M. Local Field Factors and Dielectric Properties of Liquid Benzene. *J. Phys. Chem. B* **2015**, *119*, 11839−11845.
(54) Frisch, M. J.; Trucks, G. W.; Schlegel, H. B.; Scuseria, G. E.; Robb, M. A.; Cheeseman, J. R.; Scalmani, G.; Barone, V.; Mennucci, B.; Petersson, G. A.; et al. *Gaussian 09*; Gaussian, Inc.: Wallingford, CT, 2009.
(55) Wang, J.; Wolf, R. M.; Caldwell, J. W.; Kollman, P. A.; Case, D. A. Development and Testing of a General Amber Force Field. *J. Comput. Chem.* **2004**, *25*, 1157−1174.
(56) Wang, J.; Wang, W.; Kollman, P. A.; Case, D. A. Automatic Atom Type and Bond Type Perception in Molecular Mechanical Calculations. *J. Mol. Graphics Modell.* **2006**, *25*, 247−260.
(57) Jakalian, A.; Jack, D. B.; Bayly, C. I. Fast, Efficient Generation of High-Quality Atomic Charges. AM1-BCC Model: II. Parameterization and Validation. *J. Comput. Chem.* **2002**, *23*, 1623−1641.
(58) Caleman, C.; van Maaren, P. J.; Hong, M.; Hub, J. S.; Costa, L. T.; van der Spoel, D. Force Field Benchmark of Organic Liquids: Density, Enthalpy of Vaporization, Heat Capacities, Surface Tension, Isothermal Compressibility, Volumetric Expansion Coefficient, and Dielectric Constant. *J. Chem. Theory Comput.* **2012**, *8*, 61−74.
(59) Jorgensen, W. L.; Chandrasekhar, J.; Madura, J. D.; Impey, R. W.; Klein, M. L. Comparison of Simple Potential Functions for Simulating Liquid Water. *J. Chem. Phys.* **1983**, *79*, 926−935.
(60) Hess, B.; Kutzner, C.; van der Spoel, D.; Lindahl, E. GROMACS 4: Algorithms for Highly Efficient, Load-Balanced, and Scalable Molecular Simulation. *J. Chem. Theory Comput.* **2008**, *4*, 435−447.
(61) Böttcher, C. J. F.; van Belle, O. C.; Bordewijk, P.; Rip, A. *Theory of Electric Polarization*, 2nd ed.; Elsevier Pub. Co.: Amsterdam, The Netherlands, 1973; Vol. *1*.
(62) Saggu, M.; Levinson, N. M.; Boxer, S. G. Direct Measurements of Electric Fields in Weak OH···π Hydrogen Bonds. *J. Am. Chem. Soc.* **2011**, *133*, 17414−17419.
(63) Saggu, M.; Levinson, N. M.; Boxer, S. G. Experimental Quantification of Electrostatics in X-H···π Hydrogen Bonds. *J. Am. Chem. Soc.* **2012**, *134*, 18986−18997.
(64) Takashima, K.; Furukawa, Y. Vibrational Stark Effect (VSE) on the Infrared Spectrum of a Poly(methyl methacrylate) Thin Film. *Vib. Spectrosc.* **2015**, *78*, 54−59.
(65) Cho, M. Vibrational Solvatochromism and Electrochromism: Coarse-Grained Models and their Relationships. *J. Chem. Phys.* **2009**, *130*, 094505.
(66) Jeon, J.; Yang, S.; Choi, J.-H.; Cho, M. Computational Vibrational Spectroscopy of Peptides and Proteins in One and Two Dimensions. *Acc. Chem. Res.* **2009**, *42*, 1280−1289.
(67) Oh, K.-I.; Fiorin, G.; Gai, F. How Sensitive is the Amide I Vibration of the Polypeptide Backbone to Electric Fields? *ChemPhysChem* **2015**, *16*, 3595−3598.
(68) DeFlores, L. P.; Ganim, Z.; Ackley, S. F.; Chung, H. S.; Tokmakoff, A. The Anharmonic Vibrational Potential and Relaxation Pathways of the Amide I and II Modes of *N*-Methylacetamide. *J. Phys. Chem. B* **2006**, *110*, 18973−18980.
(69) Suzuki, E. A Quantitative Study of the Amide Vibrations in the Infra-Red Spectrum of Silk Fibroin. *Spectrochim. Acta* **1967**, *23A*, 2303−2308.
(70) Bradbury, E. M.; Elliott, A. The Infra-Red Spectrum of Crystalline *N*-Methyl Acetamide. *Spectrochim. Acta* **1963**, *19*, 995−1012.
(71) Chen, X. G.; Schweitzer-Stenner, R.; Asher, S. A.; Mirkin, N. G.; Krimm, S. Vibrational Assignments of *trans*-*N*-Methylacetamide and Some of Its Deuterated Isotopomers from Band Decomposition of IR, Visible, and Resonance Raman Spectra. *J. Phys. Chem.* **1995**, *99*, 3074−3083.
(72) Wang, Y.; Purrello, R.; Georgiou, S.; Spiro, T. G. UVRR Spectroscopy of the Peptide Bond. 2. Carbonyl H-Bond Effects on the Ground- and Excited-State Structures of *N*-Methylacetamide. *J. Am. Chem. Soc.* **1991**, *113*, 6368−6377.
(73) Hamm, P.; Lim, M.; DeGrado, W. F.; Hochstrasser, R. M. The Two-Dimensional IR Nonlinear Spectroscopy of a Cyclic Penta-Peptide in Relation to its Three-Dimensional Structure. *Proc. Natl. Acad. Sci. U. S. A.* **1999**, *96*, 2036−2041.
(74) Woutersen, S.; Hamm, P. Structure Determination of Trialanine in Water Using Polarization Sensitive Two-Dimensional Vibrational Spectroscopy. *J. Phys. Chem. B* **2000**, *104*, 11316−11320.
(75) Woutersen, S.; Hamm, P. Time-Resolved Two-Dimensional Vibrational Spectroscopy of a Short α-Helix in Water. *J. Chem. Phys.* **2001**, *115*, 7737.
(76) Torii, H.; Tasumi, M. Liquid Structure, Infrared and Isotropic/Anisotropic Raman Noncoincidence of the Amide I Band, and Low-Wavenumber Vibrational Spectra of Liquid Formamide: Molecular Dynamics and Ab Initio Molecular Orbital Studies. *J. Phys. Chem. B* **1998**, *102*, 315−321.
(77) Pawar, D. M.; Khalil, A. A.; Hooks, D. R.; Collins, K.; Elliott, T.; Stafford, J.; Smith, L.; Noe, E. A. *E* and *Z* Conformations of Esters, Thiol Esters, and Amides. *J. Am. Chem. Soc.* **1998**, *120*, 2108−2112.
(78) Wiberg, K. B.; Wong, M. W. Solvent Effects. 4. Effect of Solvent on the *E*/*Z* Energy Difference for Methyl Formate and Methyl Acetate. *J. Am. Chem. Soc.* **1993**, *115*, 1078−1084.
(79) Oki, M.; Nakanishi, H. Conformations of the Ester Group. *Bull. Chem. Soc. Jpn.* **1970**, *43*, 2558−2566.
(80) Candelaresi, M.; Pagliai, M.; Lima, M.; Righini, R. Chemical Equilibrium Probed by Two-Dimensional IR Spectroscopy: Hydrogen Bond Dynamics of Methyl Acetate in Water. *J. Phys. Chem. A* **2009**, *113*, 12783−12790.
(81) Pagliai, M.; Muniz-Miranda, F.; Cardini, G.; Righini, R.; Schettino, V. Hydrogen Bond Dynamics of Methyl Acetate in Methanol. *J. Phys. Chem. Lett.* **2010**, *1*, 2951−2955.
(82) Kashid, S. M.; Jin, G. Y.; Bagchi, S.; Kim, Y. S. Cosolvent Effects on Solute-Solvent Hydrogen-Bond Dynamics: Ultrafast 2D IR Investigations. *J. Phys. Chem. B* **2015**, *119*, 15334−15343.
(83) Olivato, P. R.; Guerrero, S. A.; Yreijo, M. H.; Rittner, R.; Tormena, C. F. Conformational and Electronic Interaction Studies of 2-Fluoro-Substituted *N*,*N*-Dimethylacetamides. *J. Mol. Struct.* **2002**, *607*, 87−99.

DOI: 10.1021/acs.jpcb.6b08133
J. Phys. Chem. B 2016, 120, 9672−9684

(84) Katsumoto, Y.; Tanaka, T.; Ozaki, Y.; Hosoi, S. Effects of Dipole Interaction and Solvation on the C═O Stretching Band of *N,N*-Dimethylacetamide in Nonpolar Solutions: Infrared, Isotropic and Anisotropic Raman Measurements. *Vib. Spectrosc.* **2009**, *51*, 119−124.
(85) Thomas, H. D.; Jonas, J. High Pressure Raman Study of the CO Stretching Mode in Liquid *N,N*-Dimethylacetamide. *J. Chem. Phys.* **1989**, *90*, 4144−4149.
(86) Lee, H.; Choi, J.-H.; Cho, M. Vibrational Solvatochromism and Electrochromism. II. Multipole Analysis. *J. Chem. Phys.* **2012**, *137*, 114307.
(87) Błasiak, B.; Cho, M. Vibrational Solvatochromism. II. A First-Principle Theory of Solvation-Induced Vibrational Frequency Shift Based on Effective Fragment Potential Method. *J. Chem. Phys.* **2014**, *140*, 164107.
(88) Błasiak, B.; Lee, H.; Cho, M. Vibrational Solvatochromism: Towards Systematic Approach to Modeling Solvation Phenomena. *J. Chem. Phys.* **2013**, *139*, 044111.
(89) Wang, L.; Middleton, C. T.; Zanni, M. T.; Skinner, J. L. Development and Validation of Transferable Amide I Vibrational Frequency Maps for Peptides. *J. Phys. Chem. B* **2011**, *115*, 3713−3724.
(90) DeCamp, M. F.; DeFlores, L.; McCracken, J. M.; Tokmakoff, A.; Kwac, K.; Cho, M. Amide I Vibrational Dynamics of *N*-Methylacetamide in Polar Solvents: The Role of Electrostatic Interactions. *J. Phys. Chem. B* **2005**, *109*, 11016−11026.
(91) Fried, S. D.; Boxer, S. G. Electric Fields and Enzyme Catalysis. *Annu. Rev. Biochem.* **2017**, *86*, submitted for publication.
(92) Warshel, A. Energetics of Enzyme Catalysis. *Proc. Natl. Acad. Sci. U. S. A.* **1978**, *75*, 5250−5254.
(93) Warshel, A. Electrostatic Origin of the Catalytic Power of Enzymes and the Role of Preorganized Active Sites. *J. Biol. Chem.* **1998**, *273*, 27035−27038.
(94) Warshel, A.; Sharma, P. K.; Kato, M.; Xiang, Y.; Liu, H.; Olsson, M. H. Electrostatic Basis for Enzyme Catalysis. *Chem. Rev.* **2006**, *106*, 3210−3235.
(95) Fried, S. D.; Boxer, S. G. Response to Comments on "Extreme Electric Fields Power Catalysis in the Active Site of Ketosteroid Isomerase". *Science* **2015**, *349*, 936.
(96) Reichardt, C.; Welton, T. *Solvents and Solvent Effects in Organic Chemistry*, 3rd ed.; Wiley-VCH: Weinheim, Germany, 2010.
(97) Hamed, R. B.; Batchelar, E. T.; Clifton, I. J.; Schofield, C. J. Mechanisms and Structures of Crotonase Superfamily Enzymes - How Nature Controls Enolate and Oxyanion Reactivity. *Cell. Mol. Life Sci.* **2008**, *65*, 2507−2527.
(98) Benning, M. M.; Taylor, K. L.; Liu, R.-Q.; Yang, G.; Xiang, H.; Wesenberg, G.; Dunaway-Mariano, D.; Holden, H. M. Structure of 4-Chlorobenzoyl Coenzyme A Dehalogenase Determined to 1.8 Å Resolution: An Enzyme Catalyst Generated via Adaptive Mutation. *Biochemistry* **1996**, *35*, 8103−8109.
(99) Zheng, Y.-J.; Bruice, T. C. On the Dehalogenation Mechanism of 4-Chlorobenzoyl CoA by 4-Chlorobenzoyl CoA Dehalogenase: Insights from Study Based on the Nonenzymatic Reaction. *J. Am. Chem. Soc.* **1997**, *119*, 3868−3877.
(100) Warshel, A. How Do Serine Proteases Really Work? *Biochemistry* **1989**, *28*, 3629−3637.
(101) Schutz, C. N.; Warshel, A. The Low Barrier Hydrogen Bond (LBHB) Proposal Revisited: The Case of the Asp···His Pair in Serine Proteases. *Proteins: Struct., Funct., Genet.* **2004**, *55*, 711−723.
(102) Wilmouth, R. C.; Edman, K.; Neutze, R.; Wright, P. A.; Clifton, I. J.; Schneider, T. R.; Schofield, C. J.; Hajdu, I. X-Ray Snapshots of Serine Protease Catalysis Reveal a Tetrahedral Intermediate. *Nat. Struct. Biol.* **2001**, *8*, 689−694.
(103) Frey, P. A.; Whitt, S. A.; Tobin, J. B. A Low-Barrier Hydrogen Bond in the Catalytic Triad of Serine Proteases. *Science* **1994**, *264*, 1927−1930.

DOI: 10.1021/acs.jpcb.6b08133
J. Phys. Chem. B 2016, 120, 9672−9684

Supplementary Information for

Vibrational Stark Effects of Carbonyl Probes Applied to Reinterpret IR and Raman Data for Enzyme Inhibitors in Terms of Electric Fields at the Active Site

Samuel H. Schneider and Steven G. Boxer*

Department of Chemistry, Stanford University, Stanford, California 94305–5012, United States

* Corresponding author. E-mail: sboxer@stanford.edu

Contents

1. Supplementary Figures

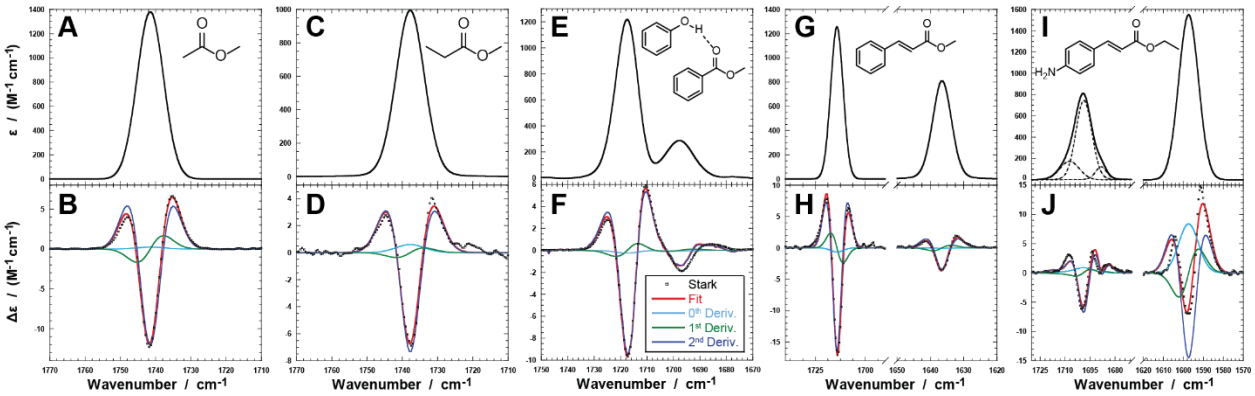

Figure S1. Infrared absorption and Stark spectra for various oxoester compounds. The infrared absorption spectrum of the C=O stretch of (A) 50 mM methyl acetate, (C) 50 mM methyl propionate, (E) 150 mM methyl benzoate in the presence of 50 mM phenol, (G) 100 mM methyl *trans*-cinnamate (C=C stretch on right, $\bar{\nu}$=1636.5 cm^{-1}, ε_{max}=811 M^{-1} cm^{-1}, FWHM=6.6 cm^{-1}), and (I) 100 mM ethyl 4-aminocinnamate (C-N stretch on right, $\bar{\nu}$=1597.2 cm^{-1}, ε_{max}=1550 M^{-1} cm^{-1}, FWHM=11.7 cm^{-1}) in glass forming solvents at 77K. The corresponding Stark spectrum (■) of (B) methyl acetate, (D) methyl propionate, (F) methyl benzoate, (H) methyl *trans*-cinnamate ($|\Delta\vec{\mu}_{C=C}|f$ =0.58 cm^{-1}/(MV/cm)), and (J) ethyl 4-aminocinnamate ($|\Delta\vec{\mu}_{C-N}|f$=1.51 cm^{-1}/(MV/cm)) in glass-forming solvents at 77K scaled to 1.0 MV/cm with fit (red) and derivative contributions (cyan, green, blue). Dashed lines are Voigt profiles fit to the absorbance spectrum.

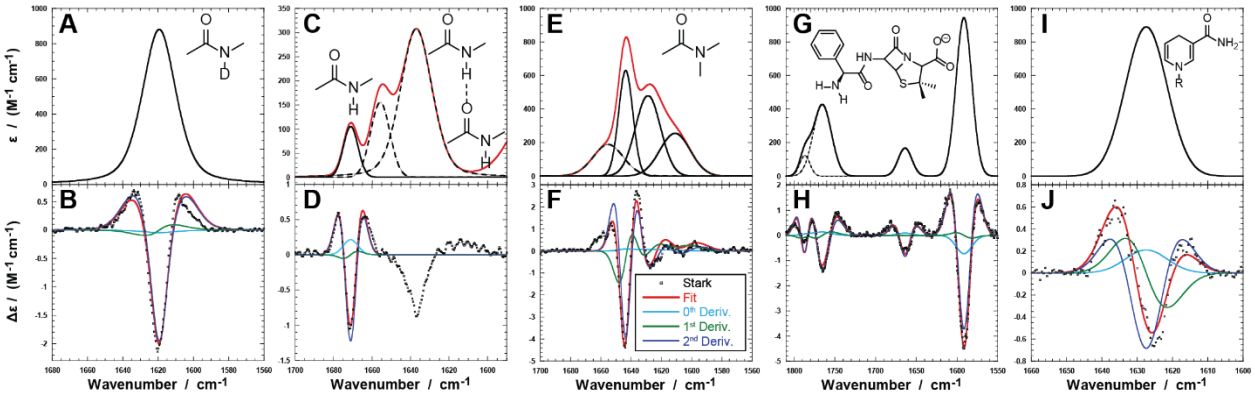

Figure S2. Infrared absorption and Stark spectra for various amide compounds. The infrared absorption spectrum of the C=O stretch of (A) 200 mM *N*-methylacetamide (N-deuterated), (C) 100 mM *N*-methylacetamide, (E) 100 mM *N*,*N*-dimethylacetamide, (G) 100 mM ampicillin (asymmetric COO^- stretch on far right, $\bar{\nu}$=1591.5 cm^{-1}, ε_{max}=945 M^{-1} cm^{-1}, FWHM=22.9 cm^{-1}), and (I) 93 mM NADPH in glass forming solvents at 77K. The corresponding Stark spectrum (■) of (B) *N*-methylacetamide, (D) *N*-methylacetamide, (F) *N*,*N*-dimethylacetamide, (H) ampicillin ($|\Delta\vec{\mu}_{COO-}|f$ =1.93 cm^{-1}/(MV/cm)), and (J) NADPH in glass-forming solvents at 77K scaled to 1.0 MV/cm with fit (red) and derivative contributions (cyan, green, blue). The Stark spectra were fit using only the solid black Voigt profiles as shown in (C), (E), and (G) while the red line is the full absorbance spectra with corresponding peaks shown in either solid or dashed traces.

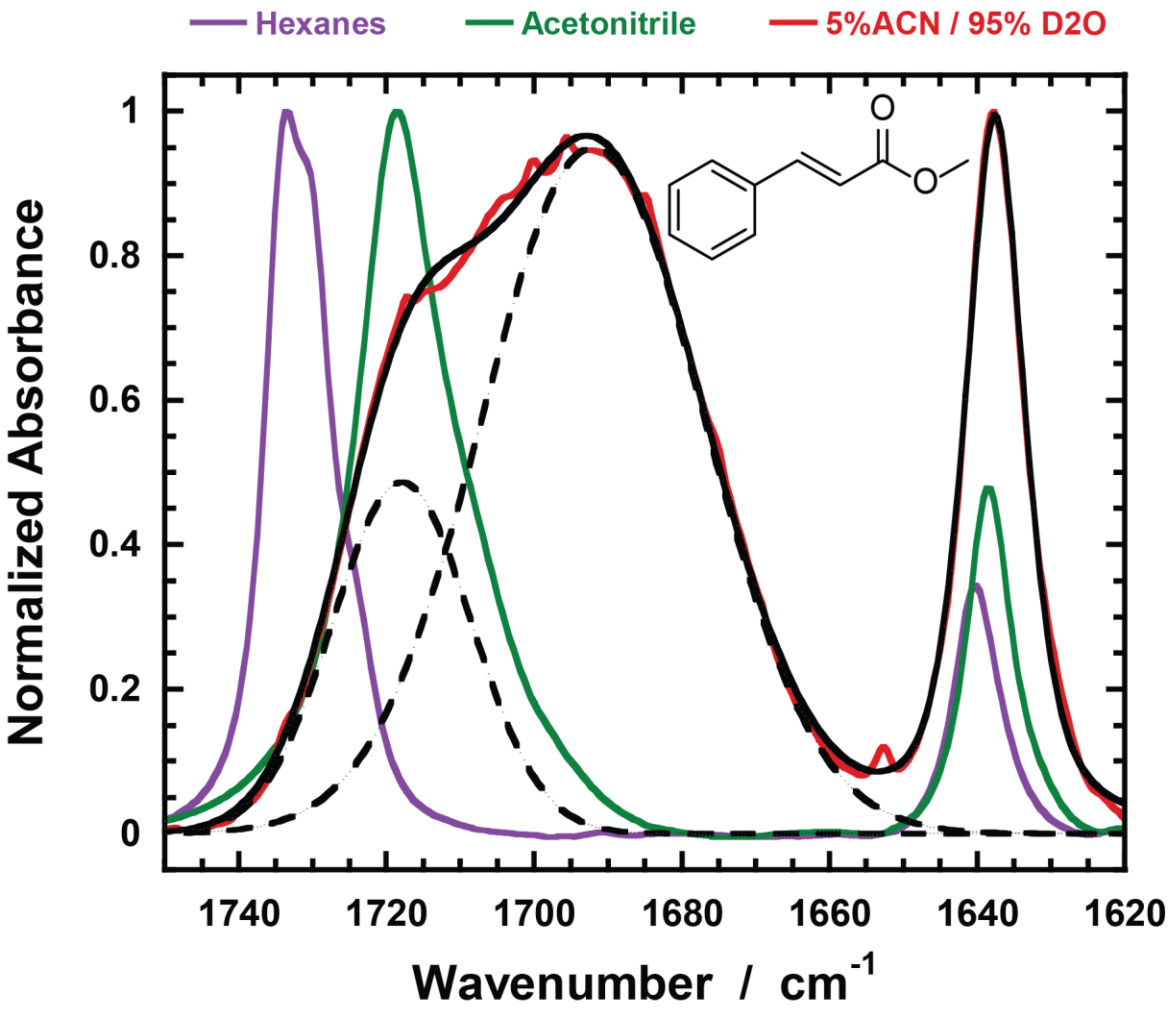

Figure S3. Vibrational solvatochromism of methyl *trans*-cinnamate. Infrared spectra of approximately 10 mM methyl *trans*-cinnamate in hexanes, acetonitrile, and 5% acetonitrile/ 95% D_2O due to poor water solubility. The broad acetonitrile/D_2O lineshape can be fit to two peaks (dashed curves) that correspond to the carbonyl in acetonitrile (1719 cm^{-1}) and D_2O (1692 cm^{-1}). Note the solvatochromic shift in the C=C mode at ca. 1640 cm^{-1}.

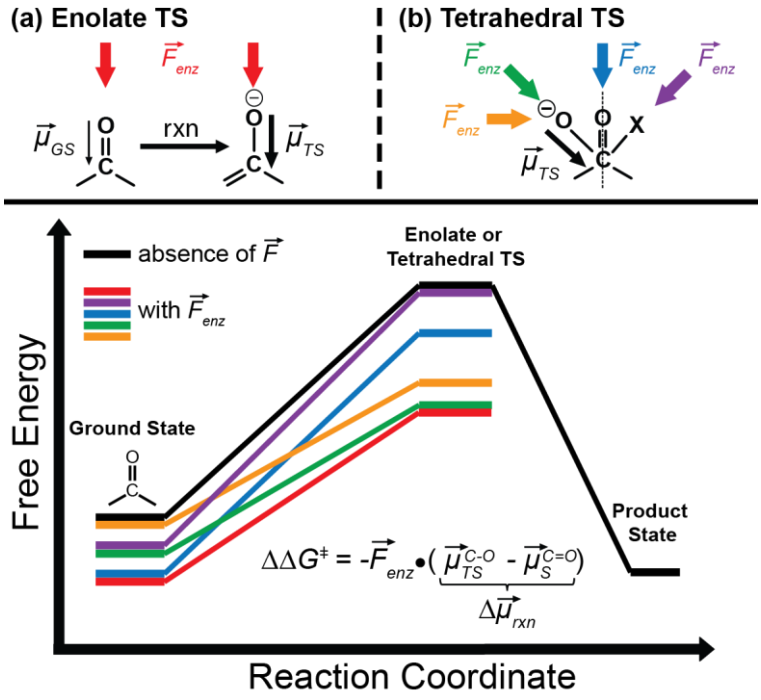

Figure S4. Effect of electric field orientation on the reaction activation barrier. For the two major classes of carbonyl chemical reactions, where the transition state is either an (a) enolate or (b) tetrahedral geometry, the possible effects of an enzyme's electric field orientation (colored arrows) on a reaction can be understood in terms of $\Delta\Delta G^{\ddagger}$. The direction of the arrows is a simplified representation of possible directions of the enzyme electric field relative to the ground state (C=O) and transition state (C-O$^-$) dipoles ($\vec{\mu}$). The effect of these different orientations on $\Delta\Delta G^{\ddagger}$ are depicted, where the rate enhancements decrease in the order of orange, green, red, blue, purple. The black lines represent the situation in the absence of a field from the enzyme, and we do not consider any effect on the product state.

Expanding upon the discussion in the main text, a change in orientation of the bond axis over the reaction coordinate provides a potential mechanism by which an enzyme can achieve large rate enhancements in terms of $\Delta\Delta G^{\ddagger} = -\vec{F}_{enz} \bullet \left(\vec{\mu}_{TS}^{C-O} - \vec{\mu}_{S}^{C=O}\right)$. Among reactions containing carbonyl substrates, many of the transition states can be classified as either enolate (Figure S4a) or tetrahedral (Figure S4b) geometries. In the former, as exemplified in KSI and Dehalogenase, the orientation of the C-O bond axis is approximately the same in the ground and transition states, and thus has the same projection of the active site electric field (red). As such, the enzyme can only lower the activation free energy by increasing the active site electric field and exploit the generally larger magnitude of $\vec{\mu}_{TS}^{C-O}$ relative to $\vec{\mu}_{S}^{C=O}$. In contrast, we can consider a reaction that proceeds through a tetrahedral transition state, simplified in Figure S4b as a displacement in the plane of the molecule; though this is not necessarily true we use this to keep the picture as simple as possible. The relative change in orientation between the C=O and C-O$^-$ bond axes provides the enzyme with a possibility to discriminate how the transition state and ground state are affected beyond a difference in the magnitude of their respective dipoles.

This effect of the orientation of the enzymes electric field with respect to the ground and transition state dipoles can be visualized in the simple model in Figure S4b, where the colored arrows denote the relative orientation of the enzyme active site's electric field with respect to the

ground and transition state bond axes. As shown in the lower part of the figure, in the case of an electric field oriented along the transition state dipole (green), one expects a preferential stabilization of the transition state, though there will still be some ground state stabilization, reducing the activation barrier. In the case of the electric field oriented perpendicular to the ground state carbonyl (orange), there will be no ground state stabilization and all of the rate enhancement will arise from transition state stabilization. An electric field that is oriented along the ground state dipole (blue), will have lower transition state stabilization, and will only facilitate catalysis if the magnitude of the transition state dipole can offset this directed stabilization of the ground state. Finally, one can imagine the anti-catalytic case in which the electric field is perpendicular to the transition state dipole (purple), and the electric field results in purely ground state stabilization.

As exemplified in this simple diagram, the evolution of an enzyme that catalyzes a reaction with a tetrahedral transition state would likely converge towards an active site electric field that lies predominantly along the transition state bond axis (orange or green). The extent to which it can preferentially stabilize the transition state relative to the ground state will reflect the preorganization of the enzyme. As described in the main text, the negative correlation observed in cysteine proteases between the C=O experienced electric field and the catalytic rate suggests that the mutations are likely altering the orientation of the enzyme electric field with respect to the acyl-intermediate probe from a geometry resembling the blue or green arrow towards orange. For serine proteases, the observed positive correlation between the active site electric field, as reported by the C=O probes, and the activation free energy may suggest that both the magnitude and orientation are altered by mutation with the active site electric field somewhere between the green and blue cases above. As such, we would hypothesize that cysteine proteases are more preorganized than serine proteases, and can fully harness these differences in the reaction coordinate for catalytic advantage. This relationship between ground and transition state stabilization likely has important consequences in binding vs. rate tradeoffs as well as protein design. Finally, we stress that these drawings are highly simplified and meant to illustrate trends; state of the art transition state and electrostatic modeling would be applied to any particular reaction to estimate the effect.

2. Supplementary Tables

Table S1. Vibrational solvatochromism and calculated electric fields from MD simulations. Peak positions as determined using either peak-picking or curve-fitting techniques and corresponding FWHM. The reported errors of the calculated electric field were determined from the correlation-adjusted error.[1]

		peak-picking	***peak-picking***	***curve-fitting***	***curve-fitting***		
substrate	**solvent**	**frequency (cm^{-1})**	**FWHM (cm^{-1})**	**frequency (cm^{-1})**	**FWHM (cm^{-1})**	**avg. electric field (MV/cm)**	**electric field std. dev. (MV/cm)**
ethyl acetate	D_2O	1703.8±0.3	35.9±0.8	1680.2±3.8 1701.9±0.1 1722.6±0.7	33.0±9.2 23.1±0.8 32.7±0.9	-67.4±1.3	22.5
	chloroform	1731.6±0.3	22.2±0.7	1710.5±0.4 1731.4±0.1	18.7±0.7 20.8±0.3	-29.3±0.7	14.1
	DCM	1733.5±0.1	16.7±1.2	1717.5±0.3 1733.5±0.2	13.8±0.8 15.7±1.2	-27.3±0.9	12.8
	DMSO	1732.7±0.1	13.6±0.1	1732.6±0.1	13.9±0.1	-26.2±0.5	11.0
	THF	1741.5±0.1	11.4±0.9	1741.5±0.2	11.0±0.2	-13.8±0.4	7.9
	dibutyl ether	1746.2±0.1	10.6±0.9	1746.3±0.1	10.5±0.1	-6.8±0.2	5.3
	Hexanes	1750.2±0.1	9.9±0.2	1750.3±0.1	9.9±0.2	-0.1±0.1	0.8
methyl benzoate	D_2O	1704.6±0.9	28.9±0.3	1686.0±1.6 1704.8±0.5	18.3±1.5 25.9±0.8	-60.3±1.6	22.1
	chloroform	1720.2±0.1	19.7±0.1	1712.0±0.2 1721.5±0.1	15.9±0.7 14.5±0.2	-22.4±1.3	13.9
	DCM	1720.6±0.1	14.4±0.1	1720.7±0.1	14.7±0.1	-22.2±0.4	12.5
	DMSO	1719.7±0.1	12.4±0.2	1719.6±0.1	12.6±0.2	-17.1±0.2	10.0
	THF	1727.5±0.4	8.0±0.8	1727.3±0.4	7.9±0.8	-9.5±0.4	7.3
	dibutyl ether	1731.4±0.4	7.4±0.1	1731.4±0.1	7.4±0.1	-4.9±0.3	5.2
	hexanes	1734.4±0.1	5.8±0.2	1734.6±0.1	5.9±0.1	-0.1±0.1	0.8
ethyl thioacetate	D_2O	1663.3±0.7	42.0±0.7	1662.6±0.2	41.5±0.5	-67.9±1.7	21.6
	chloroform	1684.9±0.2	24.7±0.1	1683.8±0.2	25.2±0.2	-27.8±0.5	13.3
	DCM	1686.8±0.1	18.7±0.4	1686.9±0.1	19.3±0.4	-25.7±0.7	12.4
	DMSO	1686.2±0.1	16.9±0.1	1685.8±0.1	17.2±0.2	-24.4±0.4	11.3
	THF	1693.9±0.1	12.9±0.4	1693.9±0.1	13.2±0.3	-12.4±0.3	8.1
	dibutyl ether	1697.8±0.1	13.1±1.0	1698.7±0.3	13.0±0.9	-5.9±0.2	5.6
	hexanes	1701.0±0.1	10.3±0.1	1701.2±0.1	10.4±0.1	-0.1±0.1	0.7
butyl thiobenzoate	1:2 (% v/v) DMSO/D_2O [a]	*****	*****	1628.3±1.9 1645.4±0.3 1662.6±0.1	34.7±2.2 19.1±0.4 17.5±0.3	-59.5±2.2 [b]	21.9 [b]
	chloroform	1659.2±0.1	19.2±3.1	1659.4±0.4	17.1±2.2	-20.2±1.2	13.6
	DCM	1660.4±0.1	18.6±0.4	1660.2±0.1	18.9±0.4	-21.0±0.2	12.2
	DMSO	1659.6±0.1	18.5±0.4	1659.9±0.2	19.3±0.4	-15.8±0.5	10.5
	THF	1666.3±0.1	9.6±0.1	1666.2±0.1	10.3±0.4	-8.9±0.2	7.4
	dibutyl ether	1670.2±0.1	9.0±0.1	1670.0±0.1	9.1±0.1	-4.2±0.4	5.1
	hexanes	1672.6±0.1	6.1±0.1	1672.5±0.1	6.1±0.1	-0.1±0.1	0.7
***N*,*N*-dimethylacetamide**	D_2O	1607.4±0.1	20.2±0.1	1607.7±0.1	20.6±0.1	-99.2±2.3	21.3
	chloroform	1633.0±0.2	24.5±1.0	1633.4±0.2 1651.2±0.8	22.1±0.8 23.7±2.1	-42.4±0.7	12.9

	DCM	1639.5±0.7	28.0±3.7	1639.3±0.3	28.2±3.5	-41.3±0.7	12.1
	DMSO	1639.8±0.2	22.7±0.9	1639.5±0.3 1653.9±4.5	19.9±0.8 24.9±3.9	-37.3±1.3	10.2
	THF	1661.6±0.6	19.7±1.4	1645.7±2.8 1652.6±0.8 1661.8±0.3	25.7±6.2 7.3±2.7 13.2±0.9	-20.9±0.7	7.4
	dibutyl ether	1668.7±0.6	13.3±0.1	1655.4±0.3 1669.0±0.2	37.2±0.4 10.5±0.1	-11.1±0.5	5.3
	hexanes	1674.1±0.1	10.3±0.2	1664.7±3.3 1674.0±0.1	34.8±1.8 9.6±0.3	-0.1±0.1	0.8

[a] 1:2 (% v/v) DMSO:D_2O was chosen as an estimate for the frequency observed in D_2O due to the poor solubility of butyl thiobenzoate in D_2O. [b] Electric fields and standard deviations correspond to those calculated in D_2O.

Table S2. Comparison of the Stark tuning rate and local field factor from VSS and field-frequency correlations.

solute	$\lvert\Delta\vec{\mu}_{C=O}\rvert f^a$ [cm^{-1}/(MV/cm)]	$\lvert\Delta\vec{\mu}_{C=O}\rvert^b$ [cm^{-1}/(MV/cm)]	f^c
ethyl acetate	1.15	0.70	1.6
ethyl thioacetate	1.47	0.56	2.6
methyl benzoate	1.15	0.48	2.4
butyl thiobenzoate	1.37	0.56	2.4
N,*N*-dimethylacetamide	1.30	0.70	1.8

[a] The Stark tuning rate as determined from vibrational Stark spectroscopy (VSS) (Table 2). [b] The Stark tuning rate as determined from correlation the slope of the field-frequency correlations (Figure 3). [c] The local field factor as determined from $\lvert\Delta\vec{\mu}_{C=O}\rvert f/\lvert\Delta\vec{\mu}_{C=O}\rvert$ from the two approaches described in the text.

3. References:

(1) Fried, S. D.; Wang, L. P.; Boxer, S. G.; Ren, P.; Pande, V. S. Calculations of the Electric Fields in Liquid Solutions. *J. Phys. Chem. B* **2013,** *117*, 16236-16248.